RESEARCH ON LAMINAR SEPARATION BUBBLES AT DELFT UNIVERSITY OF TECHNOLOGY IN RELATION TO LOW REYNOLDS NUMBER AIRFOIL AERODYNAMICS

by

J.L. van Ingen
L.M.M. Boermans

Proceedings of the Conference on Low Reynolds Number Airfoil Aerodynamics

Notre Dame, Indiana, USA
June 1985

PROCEEDINGS OF THE CONFERENCE ON LOW REYNOLDS NUMBER AIRFOIL AERODYNAMICS

Edited by
Thomas J. Mueller

UNDAS-CP-77B123
June 1985

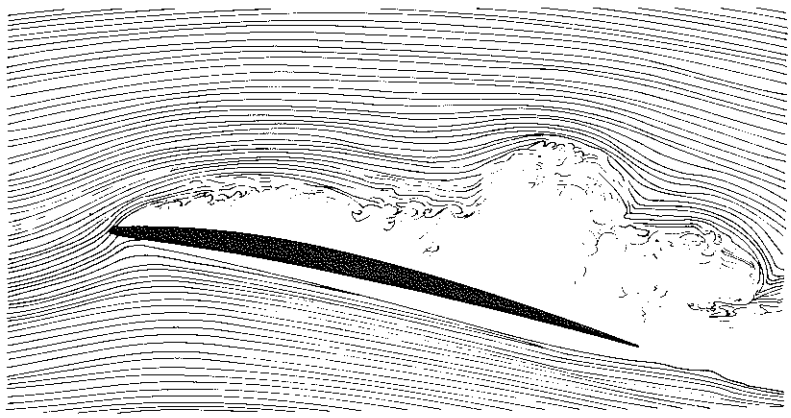

Sponsored by

NATIONAL AERONAUTICS AND SPACE ADMINISTRATION
LANGLEY RESEARCH CENTER
HAMPTON, VIRGINIA

AND

U.S. NAVY
OFFICE OF NAVAL RESEARCH
ARLINGTON, VIRGINIA

AND

THE UNIVERSITY OF NOTRE DAME
DEPARTMENT OF AEROSPACE AND MECHANICAL ENGINEERING
NOTRE DAME, INDIANA

RESEARCH ON LAMINAR SEPARATION BUBBLES AT DELFT UNIVERSITY OF TECHNOLOGY IN RELATION TO LOW REYNOLDS NUMBER AIRFOIL AERODYNAMICS

J.L. van Ingen and
L.M.M. Boermans
Department of Aerospace Engineering
Delft University of Technology
Kluyverweg 1, 2629 HS Delft, The Netherlands

ABSTRACT

This paper gives an overview of research on laminar separation bubbles at Delft University of Technology in relation to low Reynolds number airfoil aerodynamics. Results of flow visualisation studies are used to define an empirical relation for the angle γ at which the separation streamline leaves the wall. The e^n transition prediction method is extended to separated flows. It is shown that a simple bursting criterion is provided by Stratfords limiting pressure distribution for a zero skin friction turbulent boundary layer. A universal description of the laminar part of the bubble is proposed, resulting in a simple bubble prediction method. The effect of tripping devices to decrease the adverse effect of the bubble on drag is discussed. Finally some results of low Reynolds number airfoil tests are reported.

1. INTRODUCTION

At the Low Speed Laboratory (LSL) of the Department of Aerospace Engineering of the Delft University of Technology a long term research program has been going on concerning the analysis and design of airfoil sections for low speed flow. The program was started in 1966 by the first author while spending a sabbatical year at the Lockheed Georgia Research Laboratories. First results of a computer program, which used computer graphics as a novelty, have been published in [1,2,3].
This prototype program used some -at that time - readily available methods for the calculation of: the potential flow pressure distribution (conformal transformation due to Timman [4]); the laminar boundary layer (Thwaites [5]); transition (e^n method due to Smith and Gamberoni [6] and Van Ingen [7]); the turbulent boundary layer (Heads entrainment method [8]).
Very soon it became apparent that also accurate methods to calculate laminar separation bubbles were required for predicting the characteristics of airfoils at low Reynolds numbers. Research at Delft then was concentrated for some time on the laminar separation bubble [9,10,11].
A schematic description of the flowfield and the pressure distribution in the bubble region is given in fig. 1. It contains the definition of some bubble related parameters.
The present paper will focus attention on the separation region (around S); the laminar part of the bubble (S-T); transition (T) and reattachment (R). As in most engineering calculation methods we will treat the pressure distribution in the bubble as a local perturbation only of the pressure distribution curve SR which would occur for a turbulent

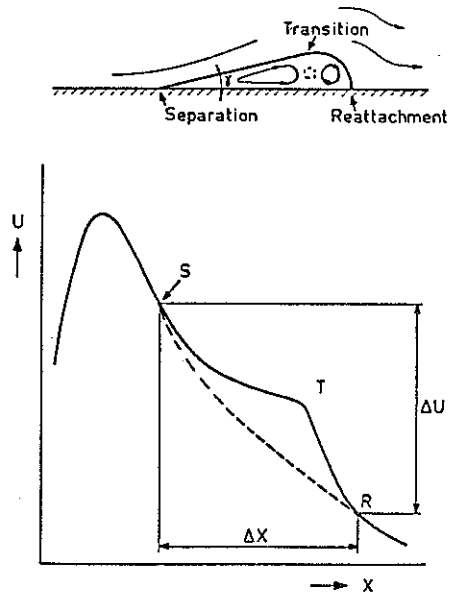

Fig. 1: Schematic diagram of flow field and pressure distribution in a laminar separation bubble.

Crabtree: $\sigma = 1 - \left(\frac{U_R}{U_S}\right)^2$

Crabtree (mod.): $\sigma_{cr} = 1 - \left(\frac{U_R}{U_T}\right)^2$

Gaster: $P = -\frac{\theta_S^2}{\nu}\frac{\Delta U}{\Delta X}$

boundary layer. Hence the laminar separation point S and the reattachment point R are thought to be on the turbulent curve. In reality a slight undershoot is often noticed, both upstream of S and downstream of R. When the flow downstream of the separation point fails to reattach, a large adverse effect on the drag and/or stalling behaviour of the airfoil is noticed. Hence an accurate prediction of this 'bursting process' is necessary.
The present status of the LSL airfoil analysis and design program may be found in [12,13]. It is being used extensively for sailplane applications [14,15,16,17].
It has been found that the effect of the laminar separation bubble on the airfoil characteristics is also due to its influence on the downstream development of the turbulent boundary layer. This effect may be noticed at chord Reynolds numbers as high as 5×10^6.
In recent years attention has been given to means to provoke earlier transition in the bubble, such that its detrimental effects are reduced. Besides conventional tripping devices, the so-called pneumatic turbulators, first used by Pfenninger [18] and rediscovered by Horstmann and Quast [19], were studied extensively in close cooperation between LSL and DFVLR Braunschweig [20].
In the present paper we will review this research at LSL related to laminar separation bubbles and its effects on airfoil characteristics at low Reynolds numbers. To keep the size of the paper within reasonable limits, the reader will have to be referred to the original papers for detailed information.

2. SOME USEFUL RELATIONS FOR SEPARATING LAMINAR FLOW

In a small neighbourhood of the separation point, where the inertial forces may be neglected, the Navier-Stokes equations admit a simple analytical solution (see [21,22,23]). Important results are:
The separation streamline leaves the wal at an angle γ (fig. 1) which is determined by:

$$\tan(\gamma) = -3 \frac{d\tau_o}{dx} \Big/ \frac{\partial p}{\partial x} \qquad (1)$$

where all quantities in (1) are evaluated at the separation point.
The equation for the streamlines (ψ = constant) reads:

$$y^2(x \tan \gamma - y) = \text{constant} \qquad (2)$$

where x is the distance downstream of separation.
The shear stress is zero at $y = y_1$ for which:

$$y_1 = \frac{1}{3} x \tan \gamma \qquad (3)$$

The velocity component u equals zero at y_2 for which:

$$y_2 = \frac{2}{3} x \tan \gamma$$

Hence (when y_3 denotes the distance to the wall of the separation streamline):

$$y_1 : y_2 : y_3 = 1 : 2 : 3 \qquad (3)$$

The pressure gradient is at an angle 1/3 γ with the wall and hence for thin bubbles, where γ is small, the pressure gradient normal to the wall is small so that the boundary layer equations might still give a reasonable result.
If we start from the boundary layer equations and assume small values of u and v we can also arrive at the previous results. Here it is assumed a priori that $\partial p/\partial x$ is indepent of y. The result (3) also follows from the expression for the velocity profile in the form:

$$\frac{u}{U} = \ell \frac{y}{\theta} + \frac{1}{2} m \left(\frac{y}{\theta}\right)^2 \qquad (4)$$

which is valid for a sufficiently small neighbourhood of the wall, not necessarily near the separation point only. From (4) it follows that the stream function ψ is given by:

$$\frac{\psi}{U\theta} = \frac{1}{2} \ell \left(\frac{y}{\theta}\right)^2 + \frac{1}{6} m \left(\frac{y}{\theta}\right)^3 \qquad (5)$$

From (5) we find that $\psi = 0$ for $y = 0$ and for:

$$y_3/\theta = -3\ell/m \qquad (6)$$

furthermore:

$$y_2/\theta = -2\ell/m \qquad (7)$$

$$y_1/\theta = -\ell/m \qquad (8)$$

Hence eq. (4) reproduces (3). In what follows we will sometimes use $g = y_3/\theta$ as shape factor for the velocity profiles with reversed flow.
An analogous behaviour is shown for solutions with reversed flow of the Falkner-Skan equation:

$$F''' + FF'' + \beta(1-F'^2) = 0 \qquad (9)$$

This equation describes the similar solutions corresponding to the pressure distribution:

$$U = u_1 x^{m_1} \qquad (10)$$

where u_1 and m_1 are constants (x is here measured from the origin of the flow.
In (9) F is the non-dimensional streamfunction, primes denote differentiation w.r.t. non-dimensional y; β is the pressure gradient parameter related to m_1 by

$$\beta = \frac{2\, m_1}{(m_1 + 1)} \qquad (11)$$

For $\beta > 0$ equation (9) only allows solutions with positive skin friction; for $0 < \beta < -.198838$ solutions with positive and negative skin friction are possible; $\beta = -0.198838$ represents the separation solution. Extensive tables of solutions with positive skin friction may be found in [24]. Some of the reversed flow solutions have been calculated first by Stewartson [25]. Table 1 gives some improved results obtained at LSL. It follows from the table that with a good approximation $y_2/y_3 = 2/3$ and $g = y_3/\theta = -3\ell/m$ as for the velocity profile (4). It should be noted that at the end of the table, corresponding to velocity profiles which

β	ℓ	m	H	L	$\frac{y_2}{y_3}$	$g = \frac{y_3}{\theta}$	$-\frac{3\ell}{m}$
-.198838	0	.06815	4.029	.8218	.667	0	0
-.18	-.0545	.05601	5.529	.7343	.667	2.917	2.920
-.10	-.0545	.01503	12.625	.3308	.678	10.665	10.000
-.05	-.0258	.00283	28.096	.1190	.698	25.748	27.350
-.025	-.0106	.00051	59.821	.0418	.721	56.478	62.353

Table 1: Some results for reversed flow solutions of eq. (9).

are found far downstream in a separation bubble, extremely large values of the shape factor H occur. This is due to the strong increase in δ^* which in turn follows from the thick region with reversed flow. Because the velocities in the separated region remain very small it may be expected that eq. (2) remains valid within a separation bubble at appreciable distances downstream of separation. This is illustrated by fig. 2 in which measured streamlines from a smoke picture of a separation bubble [10] are compared to results of a calculation using eq. (2). It should be noted that the streamlines can only be calculated when γ is known. In this case the value of γ was taken from the smoke picture.

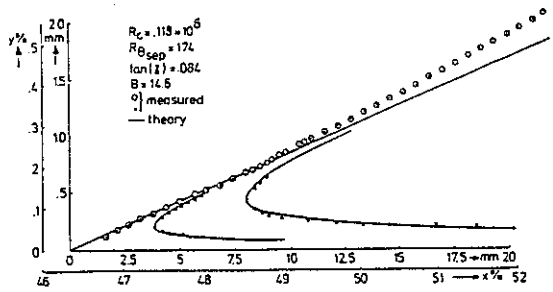

Fig. 2: Streamlines from smoke picture and comparison with equation (2).

3. RESULTS OF FLOW VISUALIZATION STUDIES OF LAMINAR SEPARATION BUBBLES

When a boundary layer calculation is performed for a prescribed pressure distribution, generally a singularity will occur at separation for which the wall shear stress τ_o tends to zero like the square root of the distance to separation (Goldstein, [26]). In this case eq. (1) would predict a separation angle γ of 90 degrees, which is obviously in contradiction with experimental evidence. Usual ways to proceed with the calculation through the separation point, are to use the Navier-Stokes equations or at least a strong interaction model coupled with the boundary layer equations.
An alternative way was followed at LSL, in order to develop an engineering method for the calculation of separation bubbles. An extensive series of flow visualization studies was made in the hope that a sufficiently general empirical relation might be found from which the separation angle γ can be determined as a function of the boundary layer characteristics upstream of separation. Once γ is known the separated flow might be calculated using simple methods.
A first series of results has been reported in [9]. Measurements were performed on seven different model configurations in three different low speed windtunnels. The flow was made visible by means of tobacco smoke introduced into the separation bubble. The shape of the front part of the bubble was determined photographically, from which the separation angle γ could be measured.
The results are shown in fig. 3, where measured values of $\tan(\gamma)$ are plotted vs. the corresponding value of R_θ at separation. It follows that a reasonably unique relation exists between γ and $(R_\theta)_{sep}$ which can be approximated by

$$\tan(\gamma) = B/(R_\theta)_{sep} \qquad (12)$$

with a value for the 'constant' B of about 15 to 20.
Later [10], similar experiments have been performed on a Wortmann FX 66-S-196V1 airfoil (series 1 in chapter 7); results are given in fig. 4. For these experiments the chord Reynolds number was reduced to such low values that bursting of the bubble occurred. It follows from fig. 4 that even after bursting relation (12) remains valid. In the LSL airfoil computer program, equation (12) is used with a constant mean value for B equal to 17.5.
When the separation streamline for a curved wall is plotted in boundary layer coordinates, where distances are measured along and normal to the

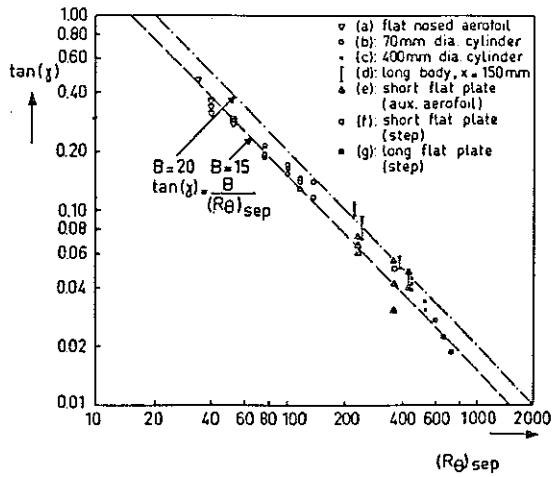

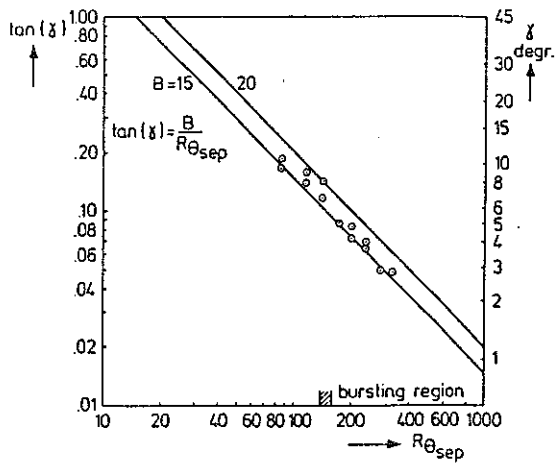

Fig. 3: Separation angles from [9]. Fig. 4: Separation angles from [10].

wall, respectively, the dividing streamline in the laminar part of the bubble is reasonably straight or slightly curved upwards (fig. 2). This finding has been used [9,10,11] to develop a simple calculation procedure for the separated laminar flow. This method employs the Von Karman momentum integral relation and the first 'compatibility condition' of the boundary layer equations. This condition relates the curvature of the velocity profile at the wall to the streamwise pressure gradient. The following additional assumptions are made.

- The angle γ can be determined from $(R_\theta)_{sep}$ by an empirical relation such as (12) with B = 17.5.
- The 'separation streamline' has a prescribed shape in the laminar part of the bubble.
- The reversed flow velocity profiles can be represented by the Stewartson second branch solutions of the Falkner-Skan equation.

It should be observed that the pressure distribution in the separated region is not given a priori but it follows from the calculations. In other words: the pressure distribution is determined such that the assumed shape of the separation streamline is compatible with the other assumptions and with the equations used. Initial conditions which are required to start the calculation at the separation point are θ and U. These conditions follow from the boundary layer calculation upstream of the separation point.
The above mentioned method has been used for some time in the LSL airfoil computer program. The resulting pressure distributions were always found to be very similar, showing the characteristic flattening in the laminar part of the bubble (fig. 1). At a later stage, the pressure distributions have been directly derived from a universal relation which is based on a combination of experimental evidence and calculations (see chapter 4).

4. A POSTULATED UNIVERSAL DESCRIPTION OF THE LAMINAR PART OF THE BUBBLE

In order to arrive at a universal model of the laminar part of the bubble we start from the boundary layer equation:

$$u \frac{\partial u}{\partial x} + v \frac{\partial u}{\partial y} = - \frac{1}{\rho} \frac{dp}{dx} + \nu \frac{\partial^2 u}{\partial y^2} \tag{13}$$

and the continuity equation:

$$\frac{\partial u}{\partial x} + \frac{\partial v}{\partial y} = 0 \tag{14}$$

It seems reasonable to assume the validity of (13) even within the separated region if only we refrain from prescribing the pressure distribution. The pressure gradient term in (13) can be related to the velocity U at the edge of the boundary layer using the Bernoulli equation.

We now make (13) and (14) non-dimensional by using θ_{sep} as a characteristic length and U_{sep} as a characteristic velocity. Taking again x as the distance downstream of separation we now define:

$$(R_\theta)_{sep} = (U_{sep}\ \theta_{sep}/\nu)$$

$$\bar{y} = y/\theta_{sep} \qquad \bar{u} = u/U_{sep} \qquad \bar{U} = U/U_{sep} \tag{15}$$

$$\xi = x/(\theta_{sep}\ R_{\theta_{sep}}) \qquad \bar{v} = (v\ R_{\theta_{sep}})/U_{sep}$$

Note that in non-dimensionalizing x and v a factor $(R_\theta)_{sep}$ has been used. This is to obtain values of ξ and $\bar{v}$ with a reasonable order of magnitude and moreover to arrive at the following equations which do not contain the Reynolds number explicitly:

$$\bar{u} \frac{\partial \bar{u}}{\partial \xi} + \bar{v} \frac{\partial \bar{u}}{\partial \bar{y}} = \bar{U} \frac{d\bar{U}}{d\xi} + \frac{\partial^2 \bar{u}}{\partial \bar{y}^2} \tag{16}$$

$$\frac{\partial \bar{u}}{\partial \xi} + \frac{\partial \bar{v}}{\partial y} = 0 \tag{17}$$

If now we make the following assumptions:

a. $\bar{U} = U/U_{sep}$ is a universal function of ξ downstream of separation.
b. All velocity profiles at separation are the same when plotted as u/U_{sep} vs y/θ_{sep}.

Then equations (16) and (17) and the corresponding boundary conditions are always the same leading to a universal solution. From this it would follow that

$$\bar{U} = U/U_{sep},\ \bar{\theta} = \theta/\theta_{sep},\ y_3/\theta_{sep} \text{ and } g = y_3/\theta$$

are universal functions of ξ. It should be stressed that the available experimental evidence to support assumption (a) is scarce and scattered. Moreover the assumption (b) may be questioned, because the various

separation profiles certainly show a variation of the shape factor H [10,27]. Nevertheless we will proceed on this line because it will lead us to a useful frame of reference to present further experimental results.
If $g = y_3/\theta$ is a universal function of ξ, then we find (note that $g = o$ at separation):

$$\tan \gamma = \left(\frac{dy_3}{dx}\right)_{x=0} = \left(\frac{dy_3}{d\xi}\frac{d\xi}{dx}\right)_{x=0} = \frac{\left(\frac{dg}{d\xi}\right)_{\xi=0}}{(R_\theta)_{sep}} \tag{18}$$

With $\left(\frac{dg}{d\xi}\right)_{\xi=0}$ equal to a universal constant, say B, we retrieve our experimental relation (12).

From a limited number of experiments we derived the following relation for $\bar{U}$ as a function of ξ:

$$\bar{U} = U/U_{sep} = 0.978 + 0.022\, e^{-4.545\,\xi - 2.5\,\xi^2} \qquad 0 \leq \xi \leq 1.3333$$

$$\bar{U} = 0.978 \qquad \xi \geq 1.3333 \tag{19}$$

Using the momentum integral relation and some relations between characteristic parameters for the Stewartson boundary layers, we derived the following relation for θ in the bubble:

$$\bar{\theta} = \theta/\theta_{sep} = \left[1 + 1.52\left(1 - (1 - 0.75\,\xi)^4\right)\right]^{1.25} \qquad 0 \leq \xi \leq 1.3333$$

$$\bar{\theta} = 1.1935 \qquad \xi \geq 1.3333 \tag{20}$$

Both equations (19) and (20) are at present used as a standard in the LSL airfoil analysis and design program. Because these relations are not based on sound theoretical or experimental evidence, it is planned to investigate the subject of the present chapter in more detail in the future.

5. THE e^n METHOD FOR TRANSITION PREDICTION

The e^n method for transition prediction for attached flows was developed in 1956 independently by Smith and Gamberoni [6] and Van Ingen [7]. The method was extended by Van Ingen to the case of suction [28] and separated flows [10,11].
The method employs linear stability theory to calculate the amplification factor σ for unstable disturbances in the laminar boundary layer (σ is defined as the natural logarithm of the ratio between the amplitude of a disturbance at a given position to the amplitude at neutral stability). It is found that at the experimentally determined transition position the calculated amplification factor for the critical disturbances attains nearly the same value (about 9) in many different cases for flows with low free stream turbulence levels. To include the effects of higher free stream turbulence levels, the critical amplification factor was made dependent on the turbulence level by Mack [29] and Van

Ingen [10,11].
To obtain the critical disturbance, calculations are made for many different disturbance frequencies; the envelope σ_a of the σ-x curves for these different frequencies is used as the critical amplification factor controlling transition. Denoting the value of σ_a at transition by n, it follows that the calculated ratio of the amplitude a of the unstable disturbances to the neutral amplitude a_o is given by:

$$a/a_o = e^n \tag{21}$$

This of course explains the name of this semi-empirical method. It is customary at LSL to use σ_a instead of n.

In linear stability theory a given two-dimensional laminar main flow is subjected to sinusoidal disturbances with a disturbance stream function:

$$\psi = \phi(y)\ e^{i(\alpha x - \omega t)} \tag{22}$$

For the spatial mode ω is real and α is complex $\alpha = \alpha_r + i\ \alpha_i$. This leads to a factor $e^{-\alpha_i x}$ in the disturbance amplitude and σ follows from:

$$\sigma = \int_{x_o}^{x} -\alpha_i\ dx \tag{23}$$

where x_o is the streamwise position where the disturbance with frequency ω is neutrally stable.
All stability data obtained from [30,31,32] and some additional inviscid stability calculations at LSL [10] (fig. 5), have been reduced to a table containing about 300 numbers.
Using this table, the amplification rate $-\alpha_i$ can easily be obtained for any velocity profile, as soon as the critical Reynolds number is known.
At LSL a boundary layer calculation method is used [10] which for attached flow is similar to Thwaites' method. It contains an extra parameter however, which makes the prediction of the separation position as accurate as for Stratford's two-layer method [33]. In separated flows an integral method is used in which the shape of the separation streamline is prescribed. Both for attached and separated flow the primary profile shape parameter is m/m_{sep}. The critical Reynolds number is a function of m/m_{sep}; this function is assumed to be equal to that obtained for the Falkner-Skan solutions.
It is clear that σ is a function of x and ω for a given boundary layer; σ can be calculated as soon as stability diagrams are available for the velocity profiles for successive streamwise positions x.
Since transition occurs in a region rather than in a point, Van Ingen introduced two values of σ_a namely σ_1 and σ_2 [10] corresponding to beginning and end of the transition region. The values of σ_1 and σ_2 depend on the free stream turbulence characteristics.
Although it is clear that the initial disturbances cannot be sufficiently characterised by the r.m.s. value of free stream turbulence alone, it

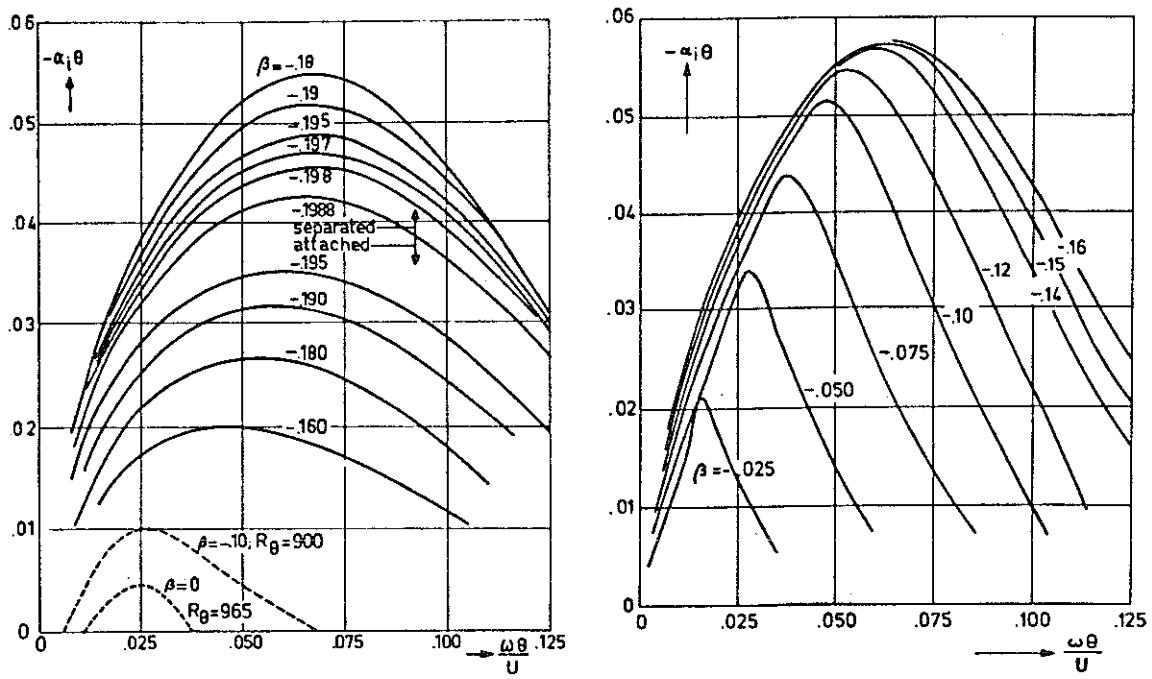

a) Attached and separated flow. b) Separated flow.

Fig. 5: Inviscid instability for Hartree's and Stewartson's velocity profiles. For attached flow $-\alpha_i\theta \to 0$ for $\beta \to 0$, for comparison the viscid instability is shown for $\beta = 0$ and -.10 when R_θ is about 1000.

may be attempted to find a relation between σ_1, σ_2 and the r.m.s. free stream turbulence Tu (in %).
In many different papers relations between Tu, R_θ or R_x at transition have been given for the flat plate. The measured transition positions may be converted to σ_a-values. Then σ_a will decrease when Tu increases; fig. 6 shows a collection of these data; for Tu > 0.1% the relation used by Mack in fig. 3 of [29] can be approximated by:

$$\sigma_1 = 2.13 - 6.18^{10}\log Tu \qquad (24)$$

while for σ_2 a reasonable approximation is:

$$\sigma_2 = 5 - 6.18^{10}\log Tu \qquad (25)$$

For values of Tu < 0.1% there is much more scatter because in this region sound disturbances may become the factor controlling transition rather than turbulence. We may also use the relations (24) and (25) for Tu < 0.1%; but then we should define an 'effective' value for Tu. Of course this does not solve the problem because we can only define an 'effective Tu' for a wind tunnel after transition experiments have been made in that same tunnel.

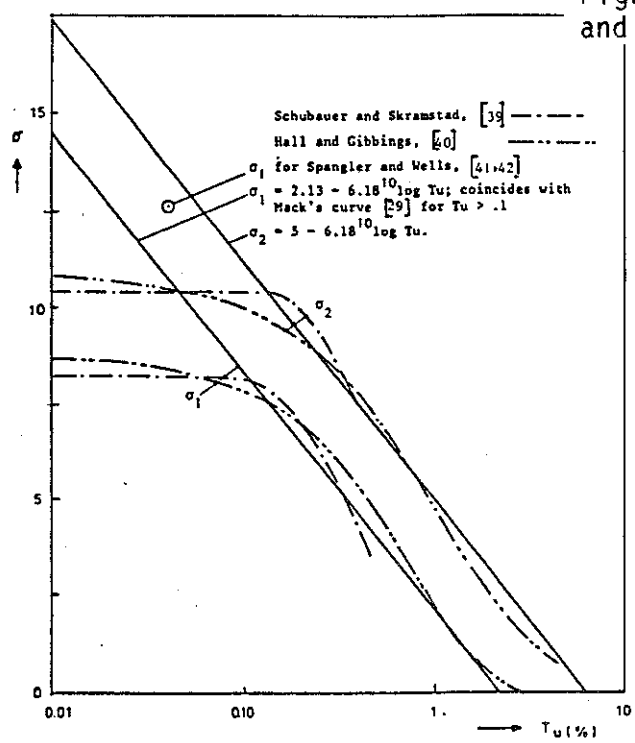

Fig. 6: Relations between σ_1, σ_2 and Tu for the flat plate.

In the LSL airfoil program we use the mean value of σ_1 and σ_2 which is called σ_{turb} to predict a 'transition point' where the turbulent boundary layer calculation is started.
The value for Tu which is used, is based on calibration calculations using available transition experiments in different wind tunnels and in free flight of gliders.
At present we use values according to table 2 [12].

Facility	Tu (%)	σ_{turb}
NACA LTT and similar tunnels	0.10	9.75
Advanced low turbulence tunnels such as at LSL	0.06	11.2
Free flight of gliders	0.014	15.0

Table 2: Tu used for different facilities.

Application of the e^n method requires the evaluation of eq. (23) for a range of reduced frequencies $\omega\nu/U_\infty^2$; this is done on a routine basis in the LSL airfoil program. For separation bubbles a short-cut method was developed [10,11] which is thought to provide a reasonably accurate first estimate of the transition position in the separated flow at rather low values of the Reynolds number, where no appreciable amplification occurs prior to separation. This short-cut method will be described in the remainder of the present chapter.

Starting from (23) and using the non-dimensional coordinate ξ we can write:

$$\sigma = \int -\alpha_i \, dx = (R_\theta)_{sep} \int \frac{-\alpha_i \theta}{\theta/\theta_{sep}} \, d\xi \tag{26}$$

The non-dimensional frequency $\omega\theta/U$ may be written as:

$$\omega\theta/U = (\omega \, \theta_{sep}/U_{sep})(\theta/\theta_{sep})(U/U_{sep})^{-1} \tag{27}$$

Then, using the results of chapter 4 that U/U_{sep}, θ/θ_{sep} and the shape factor may be taken as universal functions of ξ, it follows that for each frequency the integral in (26) is a universal function of ξ. Then, also the envelope of the integrals for the different frequencies is a universal function of ξ. Hence we can write:

$$\sigma_a = (R_\theta)_{sep} \, F(\xi) \tag{28}$$

where $F(\xi)$ is a universal function of ξ which may be determined from the known relations between ξ, g, β and the various stability data.
A simplified calculation can be made when it is assumed that in first approximation in the laminar part of the bubble θ, U and R_θ are constant and equal to their values at separation. Then constant values of $\omega\nu/U_\infty^2$ also mean constant values of $\omega\theta/U$. Furthermore it may be assumed that downstream of separation g is proportional to ξ according to

$$g = B \, \xi \tag{29}$$

Hence (26) can be written as

$$\sigma = \frac{(R_\theta)_{sep}}{B} \int (-\alpha_i \theta) \, dg \tag{30}$$

In [10] a different parameter z was used according to

$$z = g * m_{sep} \tag{31}$$

so that (30) leads to:

$$\sigma = 10^{-4} \frac{(R_\theta)_{sep}}{B \, m_{sep}} \left[10^4 \int (-\alpha_i \theta) \, dz\right] \tag{32}$$

The powers of 10 have been introduced to obtain values for the integral of a suitable order of magnitude. Similarly we can over a short interval upstream of separation, assuming ℓ to be proportional to $x_{sep}-x$, perform the integration w.r.t. ℓ instead of x.
Now we make the further assumption that the Reynolds number is so high that the stability characteristics are given with sufficient accuracy by the limiting values determined from the inviscid stability equation. Then $-\alpha_i \theta$ only depends on the value of $\omega\theta/U$ and the profile parameter β or z. Hence the integration w.r.t. z in eq. (32) can be performed once

for all independently of $(R_\theta)_{sep}$ or the pressure distribution for different values of $\omega\theta/U$. A similar result holds for the integration w.r.t. ℓ upstream of separation.
The inviscid instability for different values of β is shown in figs. 5a and 5b. Values of $10^4 \int (-\alpha_i \theta)\, dz$ are shown in fig. 7 for different values of $\omega\theta/U$ together with the envelope giving the maximum value I of the integral as a function of z. Hence the maximum amplification factor σ_a follows from (32) in the form:

$$\sigma_a = 10^{-4} \frac{(R_\theta)_{sep}}{B.m_{sep}} I \qquad (33)$$

Values of z and I for reversed flows may be found in table 3. According to previous experience with the transition prediction method it may be expected that transition will occur in practice as soon as the calculated value of σ_a exceeds a critical value which is of the order of 9, but will depend on Tu. Assuming a critical value of σ_a the transition position may be found as follows. From the known values of $(R_\theta)_{sep}$, m_{sep}, B and the critical value of σ_a we find from eq. (33) the value of I at which transition will occur. Then table 3 gives the corresponding

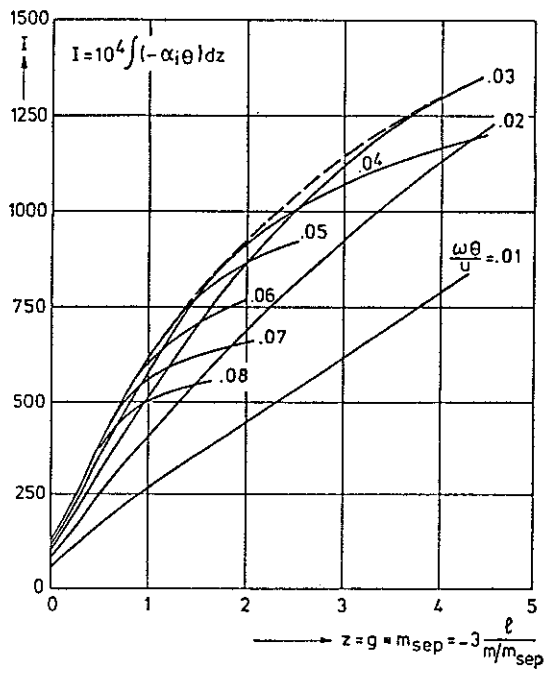

Fig. 7: Amplification integral.

β	$z=g*m_{sep}$	I
-.198838	0	127
-.198	.042	145
-.197	.061	154
-.195	.088	167
-.190	.134	190
-.180	.199	225
-.160	.307	285
-.150	.360	315
-.140	.420	348
-.120	.556	422
-.100	.682	483
-.075	1.107	659
-.050	1.864	883
-.025	4.249	1331

Table 3: z and I as a function of the Hartree shape parameter β for reversed flows.

value of $z = g * m_{sep}$; then eq. (29) and (31) determine the distance between the separation and transition points.
At LSL we use this short-cut method to obtain a first estimate of the transition position only. Subsequently we always perform the full amplification calculation where also the upstream influence is taken into account. This may lead to a shorter bubble than follows from the short-cut method.

Comparing (28) and (33) it follows that the function $F(\xi)$ is related to I according to:

$$10^4 F(\xi) = I/(B * m_{sep}) \tag{34}$$

Plots for I and $10^4 F(\xi)$ are shown in figs. 8 and 9. For small values of ξ and z we may use as a good approximation:

$$10^4 F(\xi) = 70 + 530\,\xi$$
$$I = 122.5 + 530\,z \tag{35}$$

For large values of z and ξ we may use:

$$I = 650\,\sqrt{z}$$
$$10^4 F(\xi) = 491\,\sqrt{\xi} \tag{36}$$

The linear approximation (35) will be used in chapter 7 as a frame of reference for some further experimental results.

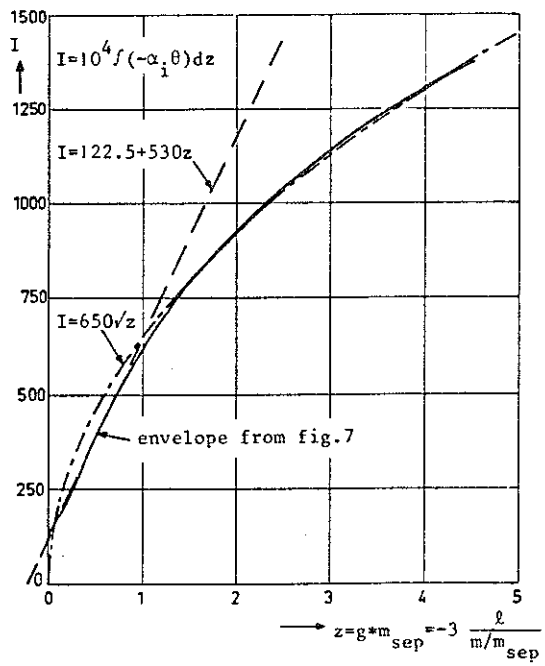

Fig. 8: The integral I and approximations (35) and (36).

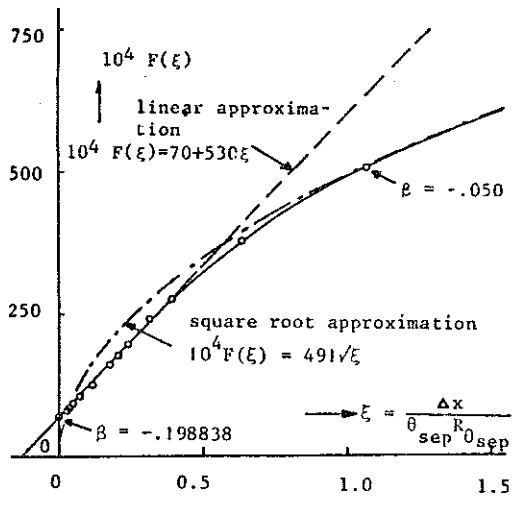

Fig. 9: The function $F(\xi)$ and approximations (35) and (36).

The square root approximation may be brought in a familiar form, which has been used by previous writers to present their experimental results. It should be noted that (36) completely neglects the amplification upstream of separation but is rather accurate for large values of z. Combining eqs. (33), (36) and (29) it follows that the position of transition x_{tr} follows from (take $x_{sep} = 0$):

$$\frac{x_{tr}}{\theta_{sep}} = \frac{\sigma_a^2\ 10^8\ B\ m_{sep}}{650^2\ (R_\theta)_{sep}} = \frac{237\ \sigma_a^2\ B\ m_{sep}}{(R_\theta)_{sep}} \tag{37}$$

Using as mean values B = 17.5 and $m_{sep} = 0.10$ we find:

$$\frac{x_{tr}}{\theta_{sep}} = \frac{415\ \sigma_a^2}{R_{\theta_{sep}}} = .0415\ \sigma_a^2\ \frac{10^4}{R_{\theta_{sep}}} \tag{38}$$

Horton [35] used the following relation

$$\frac{x_{tr}}{\theta_{sep}} = C\ \frac{10^4}{(R_\theta)_{sep}} \tag{39}$$

with values of C ranging from 3 to 5. This range of C values corresponds to σ_a values between 8.5 and 11. It should be noted that (36) and hence (39) can only be used when transition occurs rather far downstream in the bubble; that means it is a very low Reynolds number approximation. It would lead to the unrealistic result that, with increasing Reynolds number the bubble would only disappear at infinite Reynolds numbers. At the higher Reynolds numbers it should be expected that (35) is a better approximation.
It should be stressed again however that all approximations discussed in this chapter are based on the assumption that no appreciable amplification occurs upstream of separation. Only the full amplification calculation which we use in the LSL airfoil program will give a proper prediction of transition.

6. POSSIBLE METHODS TO PREDICT BURSTING OF THE BUBBLE

A number of methods may be used to predict whether reattachment of the shear layer will occur downstream of transition. A few of these methods will be briefly described in this chapter; some experimental checks will be given in chapter 7.
In [47] Crabtree observed that there seems to be a maximum limit to the pressure rise which a reattaching turbulent shear layer may overcome. From a number of experiments he deduced that the pressure coefficient

$$\sigma = 1 - \left(\frac{U_R}{U_S}\right)^2 \tag{40}$$

is nearly constant for short bubbles about to burst; the constant value he suggested was 0.35. Since it seems better to correlate different experimental results on the pressure rise between transition and reattachment we will use a slightly different coefficient σ_{cr} defined by:

$$\sigma_{cr} = 1 - \left(\frac{U_R}{U_T}\right)^2 \qquad (41)$$

If eq. (40) or (41) is to be used to predict whether reattachment will occur, the value of U_R at the possible reattachment point has to be known. In a first approximation this may be taken from the pressure distribution which would occur without the bubble being present, at the position x_{tr} (the 'inviscid pressure distribution').

In [35] Horton gave a method to predict whether and where reattachment may occur. This method is based on the simple criterion that $\left(\frac{\theta}{U}\frac{dU}{dx}\right)_r$ = constant = -.0082 for all turbulent shear layers.

Gaster [36] defined a bursting limit for the maximum value of the mean pressure gradient over the bubble - $\frac{\theta^2_{sep}}{\nu}\frac{\Delta U}{\Delta x}$ as a function of $R_{\theta_{sep}}$ (see fig. 1 and also chapter 8).

A simple criterion for bursting was found at LSL to be provided by Stratford's zero skin friction limiting pressure distribution [34]. This is the adverse pressure distribution which a turbulent boundary layer can just negotiate without separation. This limiting pressure distribution curve, starting at the measured transition point T (fig. 1) can at low Reynolds number fail to cross the 'inviscid pressure distribution curve'. This means that the requested pressure rise is more than the Stratford pressure recovery can provide and hence bursting occurs. For our experimental results on a Wortmann airfoil (chapter 7) this gave a very good prediction of the bursting Reynolds number.

In the airfoil design and analysis program at LSL we use at present the Stratford curve in a standard method to predict bursting.

7. SOME FURTHER EXPERIMENTAL RESULTS

Some further experimental results were obtained on a few different configurations [11]. In what follows these will be referred to as:

Series 1: Wortmann airfoil FX66-S-196 V1, α = 1 degr in a small noisy tunnel.

Series 2: The same Wortmann airfoil but now on a larger scale in the large low turbulence tunnel at LSL.

Series 3: A circular cylinder with a wedge-shaped tail in the large tunnel (one of the configurations of [9].

Series 4: Same as series 3 but noise from the small tunnel recorded on tape and replayed in the test section of the large low turbulence tunnel.

Fig. 10 shows pressure distributions for series 1 for various chord Reynolds numbers. Below $R_c = .118 * 10^6$ bursting is seen to occur. Separation angles γ for this case were shown in fig. 4 already. Fig. 11

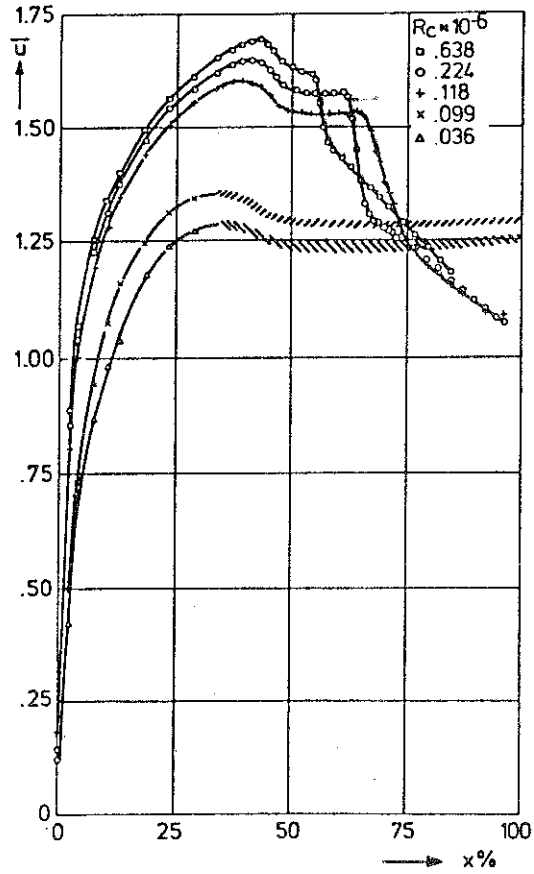

Fig. 10: Pressure distributions for series 1.

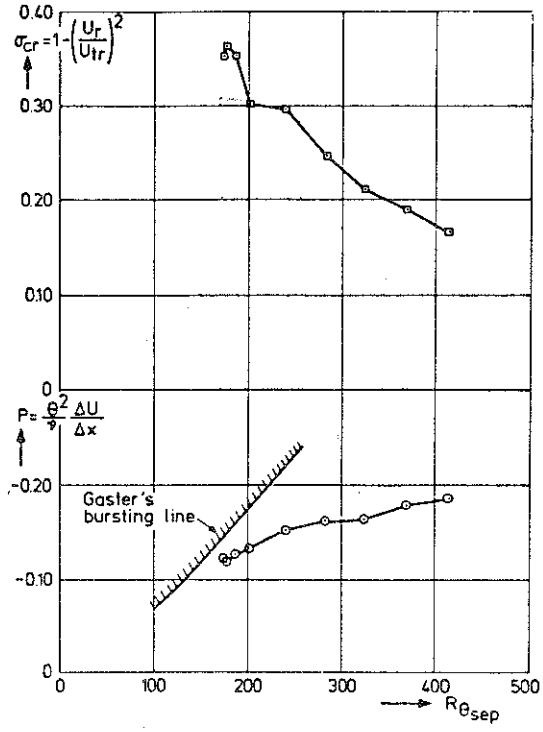

Fig. 11: Bursting parameters for series 1.

gives results for series 1, plotted in the way of Crabtree and Gaster; the figures indicate that a reasonable prediction of bursting would have resulted from both methods. Figs. 12a and 12b show the pressure distribution for the highest R_c and for the lowest Reynolds number before bursting occurs. Indicated are predictions with the method referred to in chapter 3 for B = 15 (note that at present we use B = 17.5). Furthermore the critical curves according to Horton and Stratford are indicated. Bursting occurs as soon as the critical curves do no longer cross the 'inviscid pressure distribution'. It follows that at $R_c = .118 * 10^6$ bursting is nearly reached.

The length of the laminar part of the bubble (the distance between S and T in fig. 1) is shown for all series in fig. 13, plotted in a conventional way. There is a large scatter which is partly due to experimental error but certainly also due to the different 'effective turbulence levels' Tu in the various experiments. The grid, shown in fig. 13 is based on equations (28), (35) and (25); it should represent the effect of Tu.

A better idea of the experimental scatter follows from fig. 14 where only the results for series 2 are shown. The vertical bars indicate errors in Δx of $\pm 0.5\%$ chord; hence the total length of the bar corre-

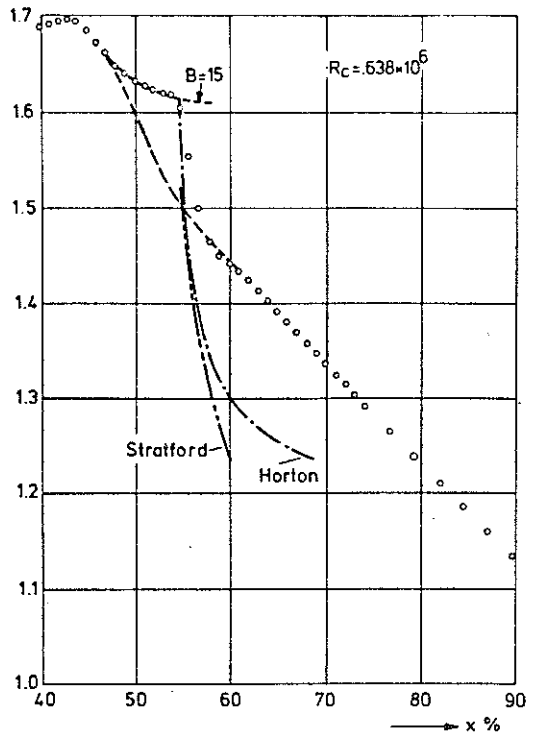

(a) $R_c = .638 * 10^6$.

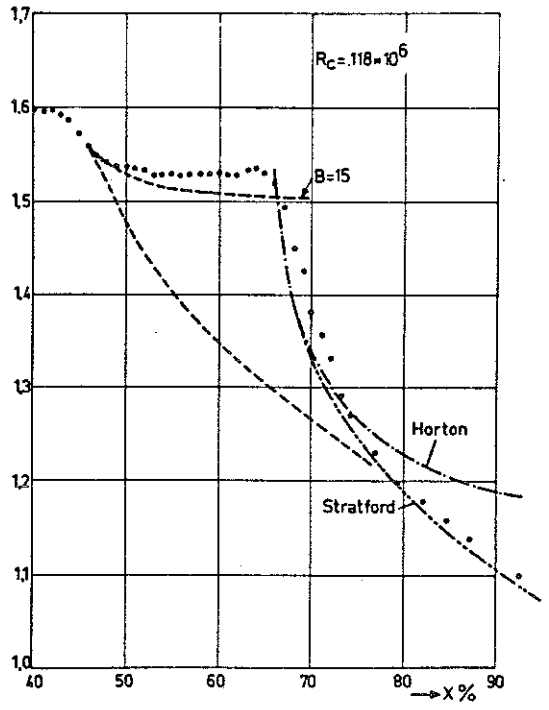

(b) $R_c = .118 * 10^6$.

Fig. 12: Pressure distributions and critical curves for bursting for two cases; series 1.

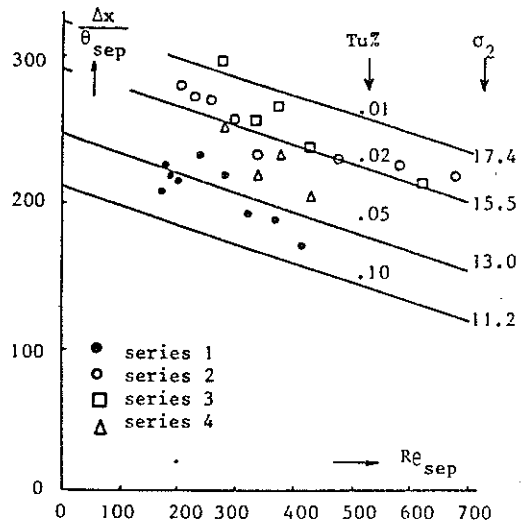

Fig. 13: Length of laminar part of the bubble; all series.

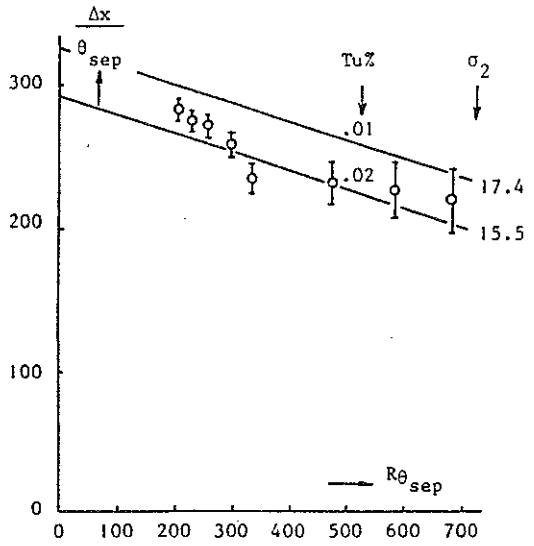

Fig. 14: Length of laminar part of the bubble; series 2.

sponds to 1% chord). With increasing $R_{\theta_{sep}}$ the scatter band widens. A better way of plotting is suggested by the linear approximation, discussed in chapter 5. As an example fig. 15 shows a replot of fig. 14 but now in the variables of chapter 5. The scatter band now has a more constant width; moreover the trend appears to be linear in accordance with the linear approximation in fig. 9 and equation (35). In fact this approximation was developed after the results of fig. 15 had been obtained. A compilation of the results for all series in the improved plot is given in fig. 16. Note that, although there remains some scatter, the experimental points seem to follow the linear trend for constant Tu (and hence constant σ_a) as indicated by equation (35).

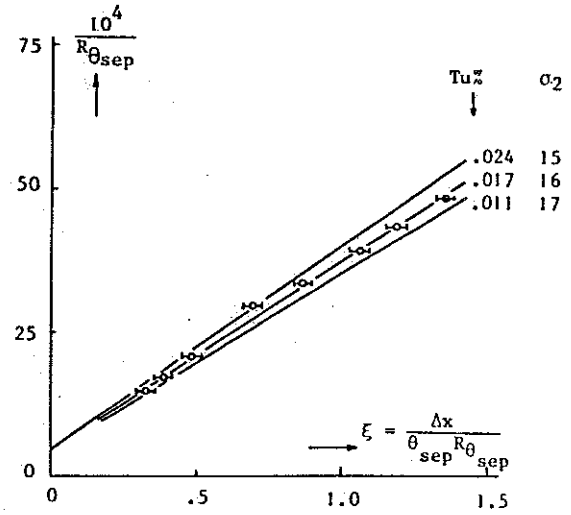

Fig. 15: Results for series 2; improved plot.

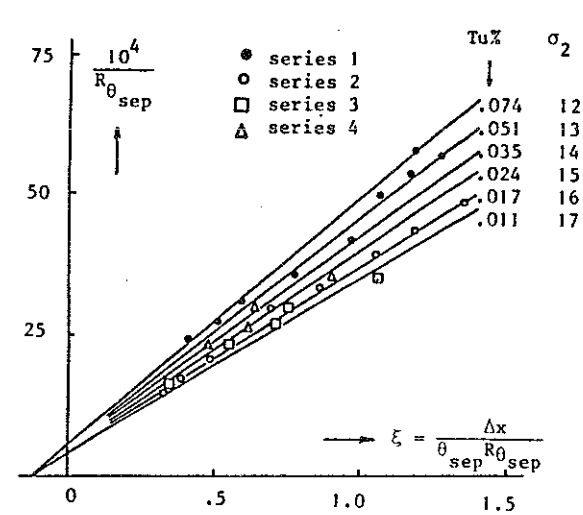

Fig. 16: Results for all series; improved plot.

8. SOME CONSEQUENCES FROM THE SIMPLE BUBBLE CALCULATION PROCEDURE

In previous chapters we derived a number of elements for a simple short-cut bubble calculation procedure using the reduced streamwise coordinate ξ. The non-dimensional edge velocity $\bar{U}$ and momentum loss thickness $\bar{\theta}$ follow from equations (19) and (20). For a given effective turbulence level Tu, the critical amplification factor follows from σ_2 using equation (25). Then the value of ξ at transition follows from (28) and (35) for a known value of $(R_\theta)_{sep}$. The Stratford limiting curve starting at T is uniquely determined by R_θ at T which follows from $\bar{U}$ and $\bar{\theta}$ at T. As an example fig. 17 shows results for Tu = 0.1%. If a linear $\bar{U}(\xi)$ distribution is assumed for the inviscid pressure distribution between S and R, possible bursting conditions follow from tangents to the Stratford curves going through S. From the points of tangency values for Crabtree's and Gasters parameters can be obtained. Note that Gasters parameter $P = -\frac{\theta_S^2}{\nu}\frac{\Delta U}{\Delta x}$ is equal to $\frac{d\bar{U}}{d\xi}$ for the linear distribution.

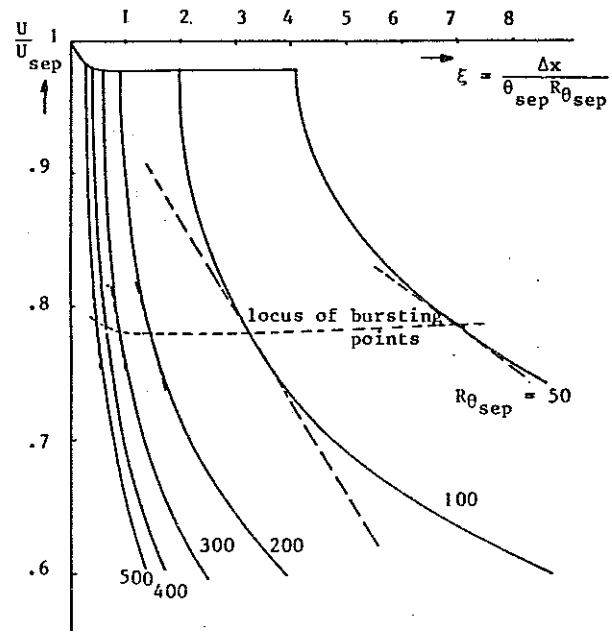

Fig. 17: Results of simple bubble calculation procedure; Tu = 0.1%.

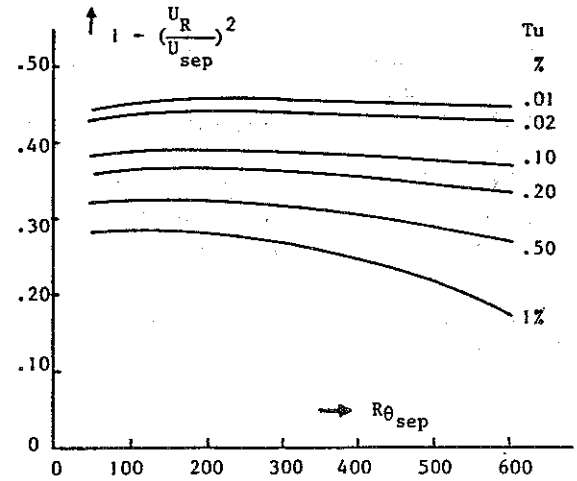

Fig. 18: Modified Crabtree parameter, eq. (41) according to the simple procedure.

Repeating this procedure for various values of Tu produced the results indicated in figs. 18 and 19. Fig. 18 gives the modified Crabtree parameter, equation (41), as a function of $(R_\theta)_{sep}$ for various Tu. It follows that indeed the pressure recovery coefficient is very nearly constant for a given value of Tu, except at the very high turbulence levels.
Fig. 19 gives Gasters parameter for various Tu as a function of $(R_\theta)_{sep}$;

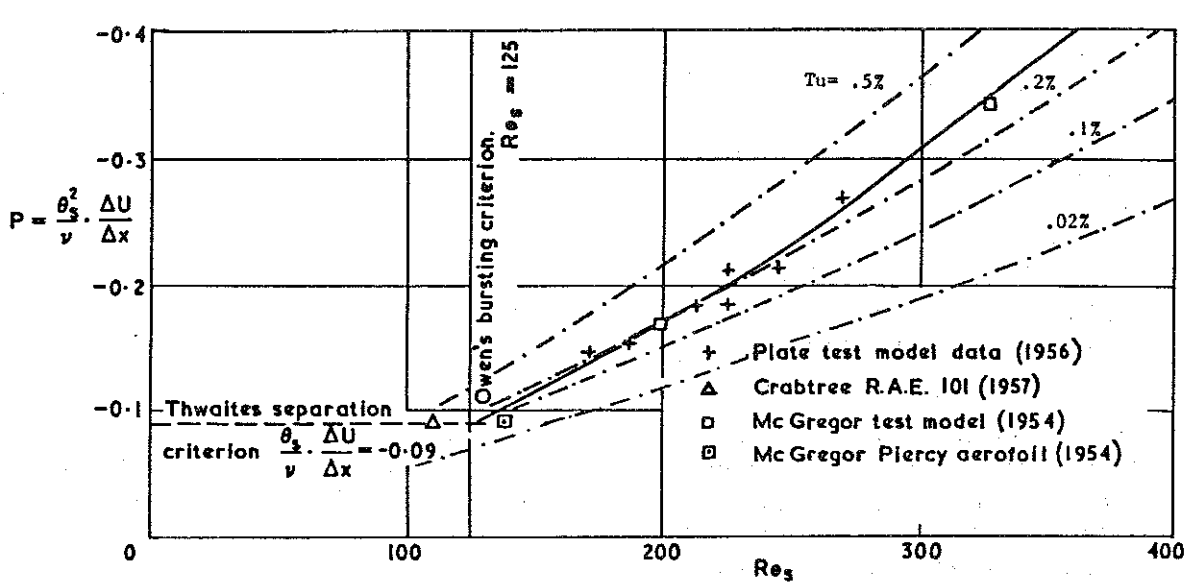

Fig. 19: Gasters bursting parameter according to the simple procedure; -.- present results for various TU.

the limiting curve given by Gaster in [36] is indicated in the figure. It follows that the present method reproduces Gasters curve for Tu about equal to 0.2%.

9. MORE DETAILED INVESTIGATIONS OF THE BUBBLE FLOW

In applications of the LSL airfoil program it was found that at low Reynolds numbers the program underestimates the airfoil drag. This is due to using improper starting conditions for the turbulent boundary layer calculation downstream of reattachment. Therefore a more detailed investigation of the flow in separation bubbles was started. Lack of space does not permit to discuss this in detail.

Some results of boundary layer measurements with a traversing total head tube for the Wortmann airfoil (series 1) are shown in fig. 20 [27]. It is seen that a strong increase of θ between T and R occurs. It also follows that early tripping of the boundary layer may reduce the downstream value of θ and hence also the drag.

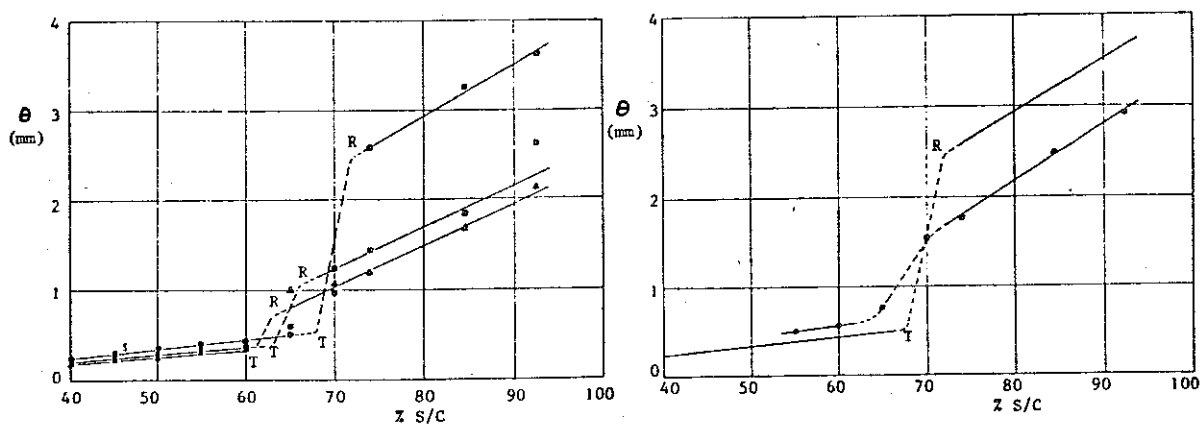

(a) $\theta(x)$ for three values of R_c; 0.154 * 10^6; 0.218 * 10^6;

(b) The effect of tripping on $\theta(x)$ at R_c = 0.154 * 10^6.

Fig. 20: Results of boundary layer measurements for the Wortmann airfoil (series 1).

Similar results for the HQ 17/14.38 airfoil, now obtained using a single hot-wire, and including turbulence intensity are shown in fig. 21a and 21b. A detailed discussion of these results may be found in [20]. Wall shear stress distributions were also obtained using Preston tubes.
Measurements with cross-wires in a boundary layer channel have shown [38] that the turbulent shear stress downstream of reattachment is much larger than would be predicted by the usual mixing length models. A research program on the development of turbulence through separation, transition and reattachment is being started at LSL.

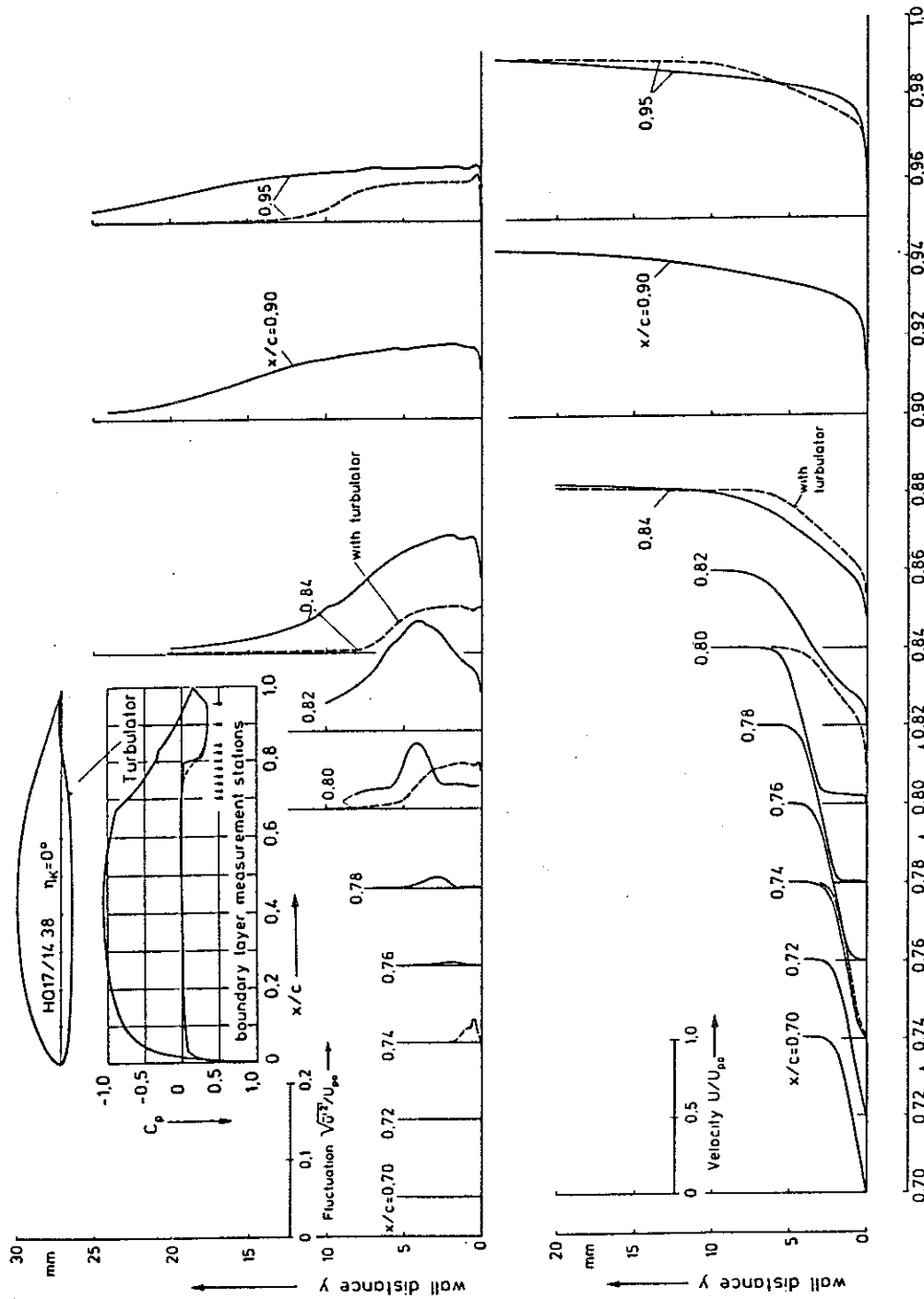

Figure 21a. Boundary layer velocity U/U_{po} and fluctuation $\sqrt{\overline{u^2}}/U_{po}$ profiles for lower surface of airfoil HQ 17/14.38 with and without laminar separation bubble, Rc = $2 \cdot 10^6$

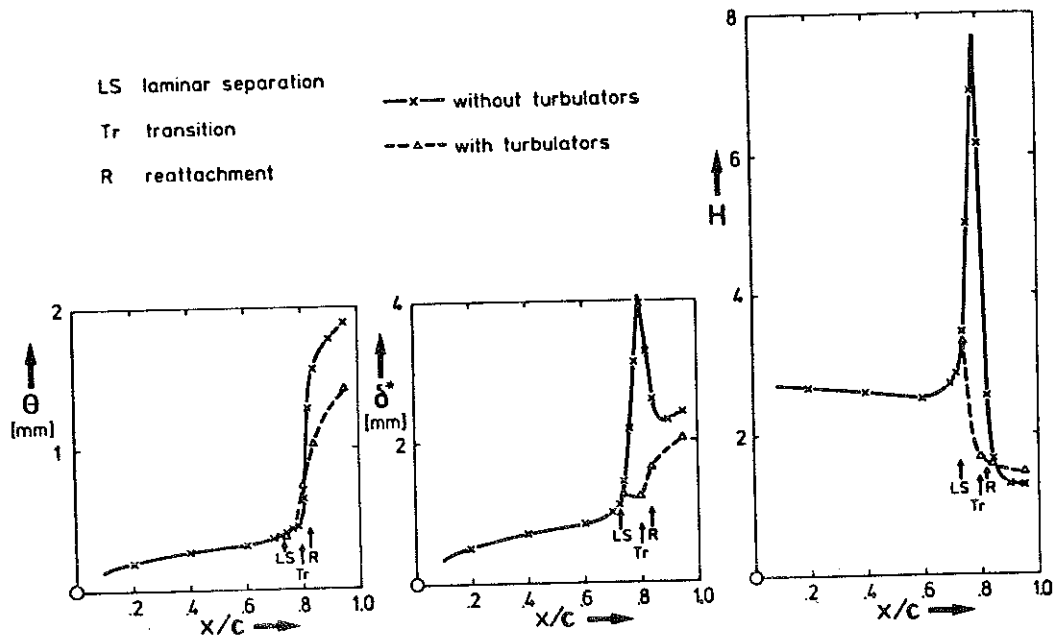

Fig. 21b: Integral boundary layer parameters for the HQ 17/14.38 airfoil; derived from fig. 21a.

10. SOME TYPICAL RESULTS OF LOW REYNOLDS NUMBER AIRFOIL TESTS

In this chapter some typical examples of experimental results are described in which laminar separation bubbles, and the elimination of them, play an important role with respect to airfoil characteristics. All measurements, ranging from $R_c = .5 * 10^5$ to $2.5 * 10^6$, were performed in the Low-Speed Low Turbulence Wind tunnel of LSL.

Fig. 22 shows the measured characteristics of a well-known airfoil designed by Eppler for model airplane application, E 205. The measuring technique is briefly described in [43]; a model with span 0.75 m and chord 0.15 m was suspended between two reflexion plates at the tips and with one tip connected to the wind tunnel balance system. The lift was measured with the balance system, the drag was measured with a wake rake connected to a sensitive Mensor Quartz manometer.

Oil flow patterns and stethoscope measurements show that the flow on the lower surface is laminar at angles of attack higher than about -2 degr. At lower angles of attack transition moves forward rapidly and a laminar separation bubble appears near the nose of the airfoil. Large laminar separation bubbles are present on the upper surface of the airfoil. For instance at $\alpha = 5$ degr. and $R_c = 1 * 10^5$ laminar separation occurs at 25% c, transition at 62% c and reattachment at 70% c. At $R_c = .6 * 10^5$ the separated boundary layer fails to reattach on the airfoil surface between $\alpha = 2$ degr and roughly 8 degr (hysteresis). At higher angles of attack there is a laminar separation bubble on the forward part of the airfoil and turbulent separation on the rearward part at all Re-numbers. The flow behaviour and characteristics of this airfoil are very similar to E 387 [43] which was also measured with a 0.6 mm trip wire positioned 10% c in front of the airfoil and 2.7% c below the chord line. This

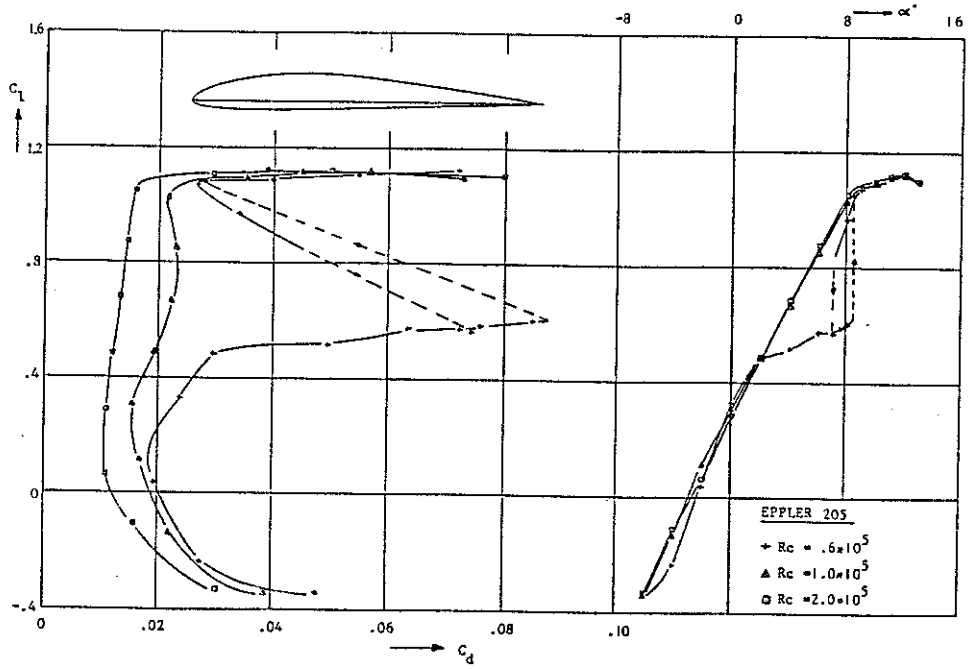

Fig. 22: Measured aerodynamic characteristics of airfoil E205.

position of the wire, which guarantees attached flow at $R_c = .6 * 10^5$, was obtained by translating the wire in front of the airfoil at several angles of attack. Similar results may be expected with a trip wire in front of airfoil E 205.

Fig. 23 shows some measured characteristics of another low Reynolds number airfoil, E 61, measured in the same way [44]. Again, the flow on the lower surface is laminar at angles of attack higher than 1 degr. At decreasing angles of attack transition moves forward rapidly and a laminar separation bubble appears on the first 20% c at 0 degr and -1 degr. At -1.5 degr angle of attack a long bubble extending to about 60% c is present. On the upper surface reattachment fails at angles of attack below about 6 degr. At 6.5 degr a laminar separation bubble is present between 50% c and 85% c while turbulent separation occurs at 95% c. At increasing angles of attack the bubble decreases in length and moves forward, as does the turbulent separation position.
To provoke transition, single frequency sound was radiated perpendicular to the upper wing surface; the sound pressure level (SPL) at the wing surface was measured at the actual wind speed. At 4.8 degr angle of attack the sound pressure level and frequency (estimated from boundary layer instability calculations first) were varied systematically. The most effective sound frequency was 300 Hz at $R_c = .8 * 10^5$ (and 145 Hz at $R_c = .5 * 10^5$). Fig. 23 shows the effect of both frequencies and SPL 104 dB on the characteristics. Fig. 24 shows an example of the effect of the sound pressure level on the lift and drag, indicating the sensitivity of the flow and hence the measured airfoil characteristics for sound disturbances in the tunnel flow.

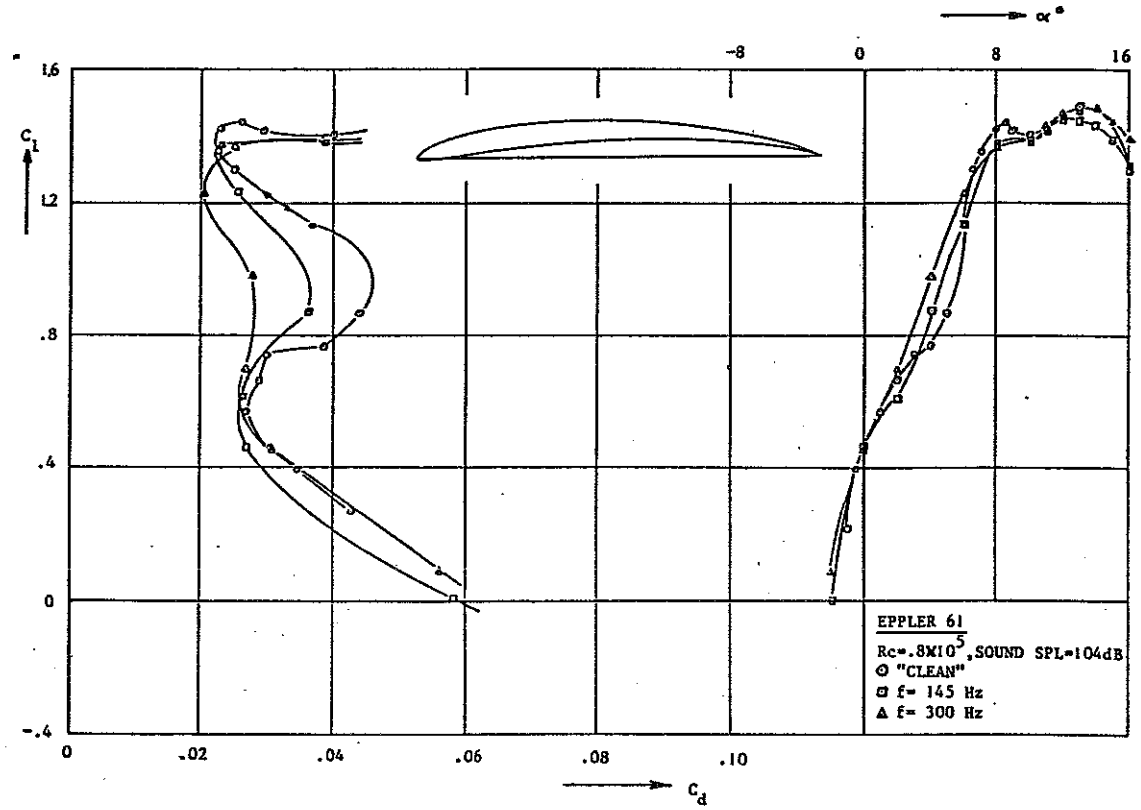

Fig. 23: Measured aerodynamic characteristics of airfoil E61 and the effect of single frequency sound disturbances.

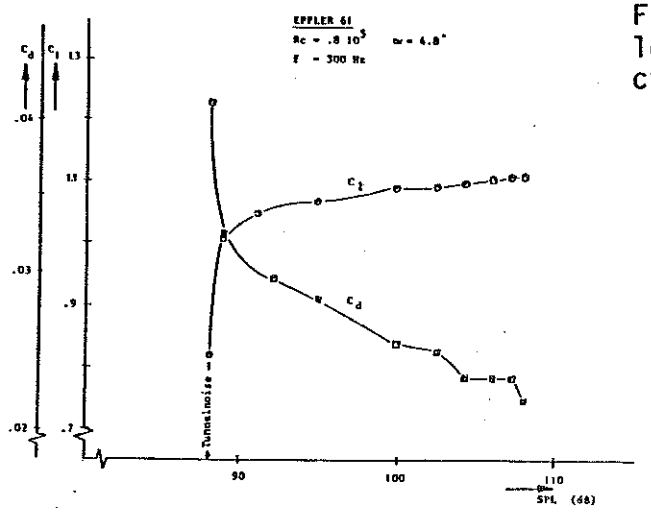

Fig. 24: Effect of sound pressure level on lift and drag coefficient of E61.

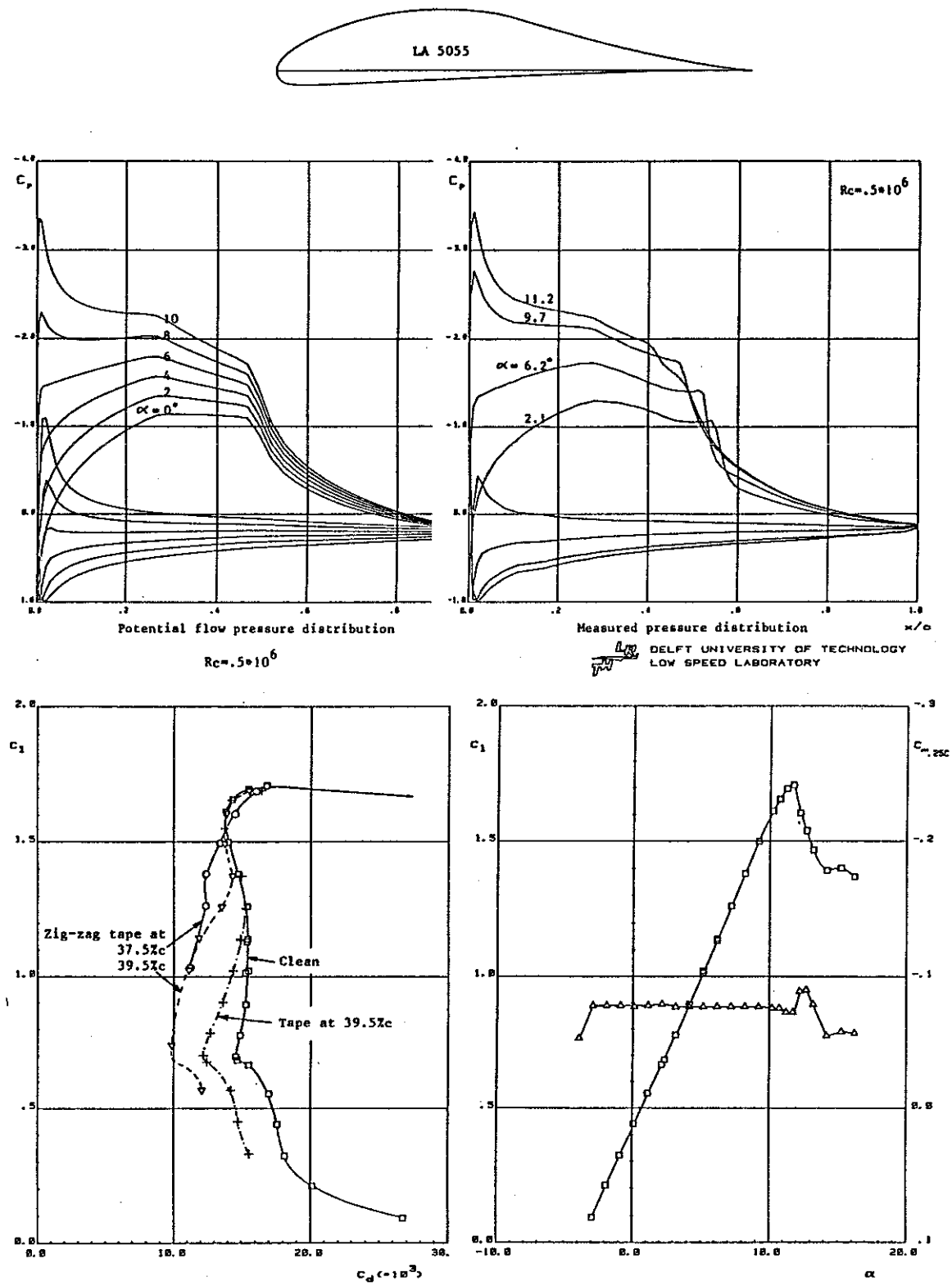

Fig. 25: Aerodynamic characteristics and pressure distributions of airfoil LA5055; effect of straight tape and zig-zag tape.

In the next examples the results were obtained by pressure measurements with models spanning the height of the wind tunnel test section (height 1.25 m, width 1.80 m).

Fig. 25 shows some results of the Liebeck LA 5055 airfoil [45]. To prevent early separation near the tunnel walls, suction was applied in a small region on the walls along the upper surface. The airfoil, designed for C_l = 1.04 at α = 4.82 degr and R_c = 0.6 * 10^6, has a distinct instability region between 27% c and 47% c upper surface, as shown in the potential flow pressure distributions. However, (detrimental) laminar separation bubbles are present at R_c = 0.5 * 10^6 (and R_c = 1 * 10^6, not shown here) as shown in the measured pressure distributions. The flow on the lower surface is laminar at angles of attack higher than 2 degr.
A strip of tape, height 0.25 mm and width 11 mm, positioned at 39.5% c, shows improvement at lift coefficients below 1.25. A zig-zag form, cut from the same tape (the idea was to strenghten the tendency of the Tollmien-Schlichting waves to become three-dimensional by matching the zig-zags to the expected spanwise wave length) shows a remarkable improvement, positioned at 39.5% c and 37.5% c. Similar results were obtained at R_c = 1 * 10^6. In fact, no better results could be obtained with tape with digged-in bumps every 5 mm span of heigth 0.65 mm or 1 mm, positioned between 39% c and 47% c.
Finally, it is mentioned that the maximum lift coefficient of 1.61 at R_c = 1 * 10^6 could be raised to 2.27 with semi triangular vortex generators [46] positioned at 20% c, despite of the very steep Stratford type pressure distribution on the rearward part of the airfoil.

Fig. 26 shows results of measurements on the DU 80-176 airfoil, designed at our institute for sailplane application [14]. Oil flow patterns indicated the absence of a laminar separation bubble on the upper surface at practical combinations of lift coefficient and Reynolds number,

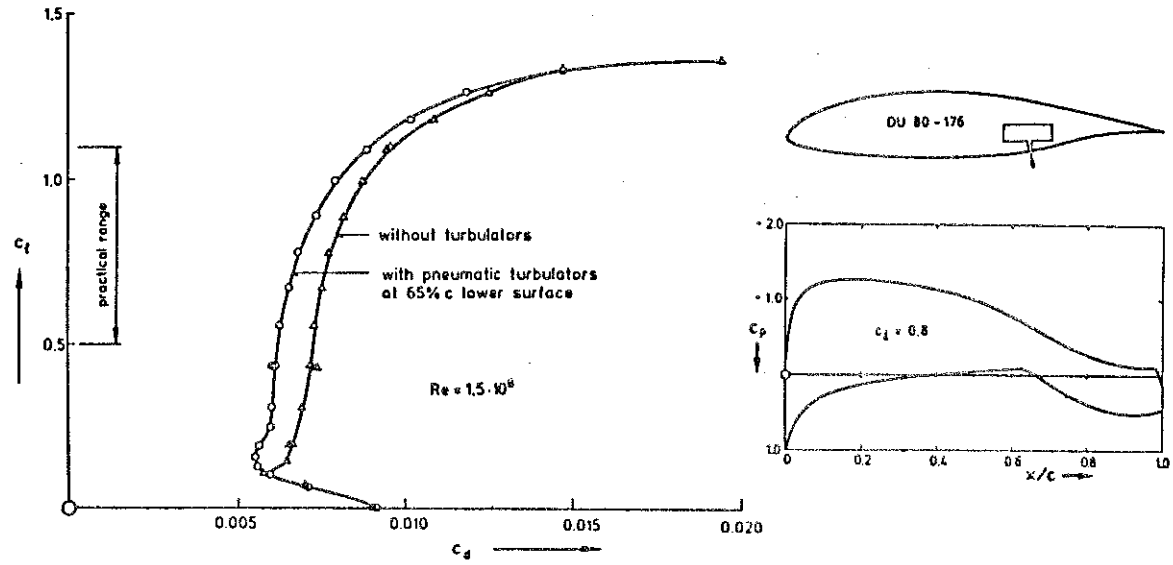

Fig. 26: Drag polars and potential flow pressure distribution of airfoil DU 80-176; effect of pneumatic turbulators.

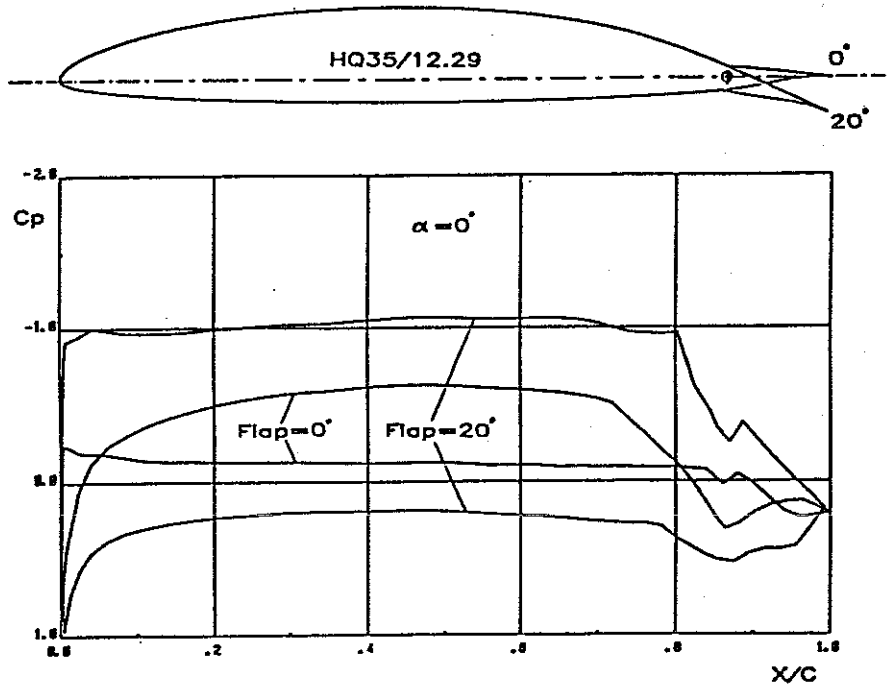

Fig. 27: Measured pressure distribution of airfoil HQ 35/12.29 (flap = 0 degr, R_c = 2 * 10^6; flap = 20 degr, R_c = 1 x 10^6.

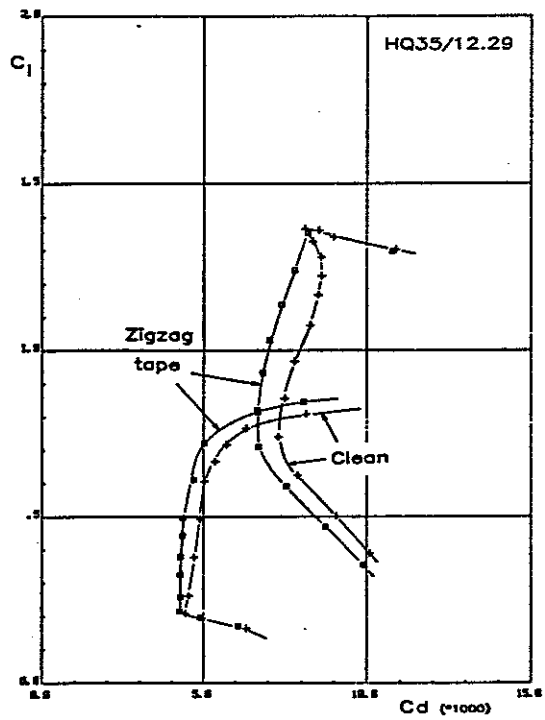

Fig. 28: Effect of zig-zag tape at 69% c upper surface and 83% c lower surface.

and the existence of a pronounced laminar separation bubble on the lower surface downstream of the pressure rise at 65% c, as intended. This bubble was eliminated and the drag reduced, fig. 26, by using pneumatic turbulators at 65% c, i.e. blowing a small amount of air through orifices periodically spaced in spanwise direction [20]. They function like roughness with adjustable height [16].
A slightly more cambered version of this airfoil was applied in modifying the wing of an existing high performance sailplane just by adding material to the surface. An air intake nozzle for each wing half with a diameter of only 6.5 mm was needed for the 870 pneumatic turbulators to do their job. Flight performance measurements before and after the wing modification showed an improvement of about 5% in glide ratio over the entire flight speed range.
Several types of high performance sailplanes are provided with pneumatic turbulators nowadays.

Another airfoil for sailplane application, HQ 35/12.29, designed by K.H. Horstmann and A. Quast of DFVLR Braunschweig (West-Germany), is shown in fig. 27. This 12.29% c thin airfoil has a camber changing flap of 13.5% chord length. In actual practice this flap extends along the whole span of the sailplane wing. Very long laminar flow regions are present on both the upper and lower surface as shown in the measured pressure distributions. Due to the stability of the laminar boundary layer and the pressure rise on the rear of the airfoil, laminar separation bubbles are present again. Fig. 28 shows the drag decrease obtained with zig-zag

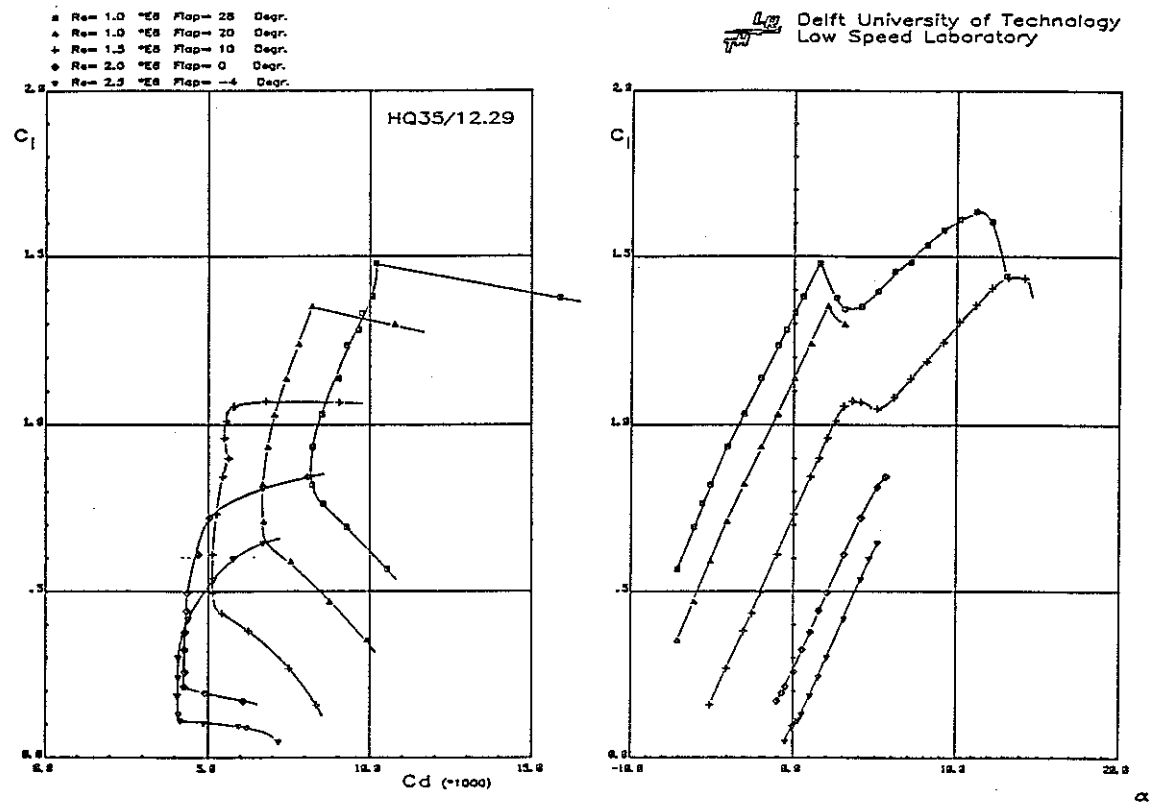

Fig. 29: Measured aerodynamic characteristics of airfoil HQ 35/12.29 with zig-zag tape at 69% c upper surface and 83% lower surface.

tape, mentioned before, at 69% c on the upper surface and 83% c on the lower surface, and fig. 29 presents the airfoil characteristics with these triggering devices at several practical combinations of Reynolds number and flap deflection.
The concave corner in the upper and/or lower surface contour at the flap hinge leads to local separation of the turbulent boundary layer. Systematically filling and rounding of this corner did not result in a drag reduction. More research is needed to exploit this phenomenon.

11. NOMENCLATURE

The symbols used are the conventional ones. Only a few are mentioned specifically below. Because the material of this paper is taken from various existing papers, some symbols have more than one meaning.

B	constant, eq. ( )
c	chord length
F	$F(\xi)$, eq. (28) and (34)
g	y_3/θ; shape parameter
H	δ^*/θ
I	envelope of $10^4 \int (-\alpha_i \theta)\, dz$
ℓ	$\tau_o \theta(uU)$
m	$-\frac{\theta^2}{\nu}\frac{dU}{dx}$
p	$-\frac{\theta_s^2}{\nu}\frac{\Delta U}{\Delta x}$, Gasters parameter, fig. 1
R_c	$U_\infty c/\nu$
R_θ	$U\theta/\nu$
s	distance along wall
Tu	turbulence level; %
U	edge velocity
U_{po}	hypothetical inviscid flow velocity at the surface
U_∞	free stream speed
$\bar{U}$	U/U_∞ in figs. 10 and 12; U/U_{sep} elsewhere
ΔU	see fig. 1
x	distance along wall, in general measured from separation point
x/c	non-dimensional distance along chord
Δx	sometimes ST in fig. 1
Δx	sometimes SR in fig. 1
y	distance from wall
y_1	y for $\tau = o$
y_2	y for $u = o$
y_3	y for separation streamline
z	$g * m_{sep}$
α	$\alpha_r + i\alpha_i$
$-\alpha_i$	spatial amplification rate

R_c	$U_\infty c/\nu$
R_θ	$U\theta/\nu$
s	distance along wall
Tu	turbulence level; %
U	edge velocity
U_{po}	hypothetical inviscid flow velocity at the surface
U_∞	free stream speed
$\bar{U}$	U/U_∞ in figs. 10 and 12; U/U_{sep} elsewhere
ΔU	see fig. 1
x	distance along wall, in general measured from separation point
x/c	non-dimensional distance along chord
Δx	sometimes ST in fig. 1
Δx	sometimes SR in fig. 1
y	distance from wall
y_1	y for $\tau = o$
y_2	y for $u = o$
y_3	y for separation streamline
z	$g * m_{sep}$
α	$\alpha_r + i\alpha_i$
$-\alpha_i$	spatial amplification rate
β	Falkner-Skan parameter
γ	separation angle (fig. 1)
δ^*	displacement thickness
θ	momentum loss thickness
$\bar{\theta}$	θ/θ_{sep}
σ	amplification factor; eq. (23)
σ_a	envelope of σ-x
σ_1	σ at beginning of transition
σ_2	σ at end of transition
σ_{turb}	$0.5(\sigma_1 + \sigma_2)$
σ	Crabtree parameter, fig. 1
σ_{cr}	modified Crabtree, fig. 1
ω	disturbance frequency
ξ	$\frac{x}{\theta_{sep}(R_\theta)_{sep}}$

Subscripts:

S, s, sep	separation
T, tr	transition
R, r	reattachment

β	Falkner-Skan parameter
γ	separation angle (fig. 1)
δ^*	displacement thickness
θ	momentum loss thickness
$\bar{\theta}$	θ/θ_{sep}
σ	amplification factor; eq. (23)
σ_a	envelope of σ-x
σ_1	σ at beginning of transition
σ_2	σ at end of transition
σ_{turb}	$0.5(\sigma_1 + \sigma_2)$
σ	Crabtree parameter, fig. 1
σ_{cr}	modified Crabtree, fig. 1
ω	disturbance frequency
ξ	$\frac{x}{\theta_{sep}(R_\theta)_{sep}}$

Subscripts:

S, s, sep	separation
T, tr	transition
R, r	reattachment

12. ACKNOWLEDGEMENTS

The authors are indebted to their collegues of the scientific, technical and administrative staff at the Department of Aerospace Engineering for their continuing support during the execution of the research program described in this paper.
They also wish to express their appreciation to DFVLR, Institut für Entwurfsaerodynamik, Braunschweig, for permission to publish the HQ 35/12.29 results which were obtained at LSL under contract with DFVLR.

13. REFERENCES

1. Cornish, J.J., 'Airfoil analysis and synthesis utilizing computer graphics', SAE Paper 670845, 1967.

2. Haas, M.E. and Ingen, J.L. van, 'Computer graphics techniques applied to airfoil design', Software Age, Vol. 1, nr 1, September 1967, pp. 34-42.

3. Ingen, J.L. van, 'Advanced computer technology in aerodynamics': a program for airfoil section design utilizing computer graphics. Lecture notes for Von Karman Institute of Fluid Dynamics (1969), AGARD lecture series no. 37 'High Reynolds-number subsonic aerodynamics', pp. 8.1-8.33, 1970.

4. Timman, R., 'The direct and inverse problem of aerofoil theory'. A method to obtain numerical solutions. National Aaerospace Laboratory NLR, Amsterdam, report NLL-F16, 1951.

5. Thwaites, B., 'Approximate calculation of the laminar boundary layer'. Aeron. Quart., 1, pp. 245-280, 1949.

6. Smith, A.M.O., Gamberoni, N., 'Transition, pressure gradient, and stability theory', Douglas Aircraft Co., report ES 26388, 1956.

7. Ingen, J.L. van, 'A suggested semi-empirical method for the calculation of the boundary layer transition region'. Delft University of Technology, Dept. of Aerospace Engineering, report VTH-74, 1956.

8. Head, M.R., 'Entrainment in the turbulent boundary layer', R and M 3152, 1958.

9. Dobbinga, E., Ingen, J.L. van, Kooi, J.W., 'Some research on two-dimensional laminar separation bubbles', AGARD CP-102, paper nr. 2, Lisbon, 1972.

10. Ingen, J.L. van, 'On the calculation of laminar separation bubbles in two-dimensional incompressible flow'. In AGARD CP-168: 'Flow Separation', Göttingen, 1975.

11. Ingen, J.L. van, 'Transition, pressure gradient, suction, separation and stability theory'. In AGARD CP-224: Laminar-Turbulent Transition, Copenhagen, 1977.

12. Ingen, J.L. van, Boermans, L.M.M. and Blom, J.J.H., 'Low speed airfoil section research at Delft University of Technology. ICAS-80-10.1, Munich, 1980.

13. Ingen, J.L. van, 'On the analysis and design of low speed airfoils using potential flow methods and boundary layer theory'. Report LR-365, Department of Aerospace Engineering, Delft University of Technology, 1982.

14. Boermans, L.M.M. and Selen, H.J.W., 'Design and tests of airfoils for sailplanes with an application to the ASW-19B'. ICAS paper 82-5.5.2, 1982.

15. Boermans, L.L.M., Selen, H.J.W. and Wijnheijmer, M.L., 'Wind tunnel tests on two wing segments of the ASW-19 sailplane'. Memorandum M-379, Delft University of Technology, Dept. of Aerospace Engineering, 1980.

16. Boermans, L.M.M. and Oolbekkink, B., 'Wind tunnel tests on an outer wing segment of the ASW-19X sailplane'. Report LR-369, Delft University of Technology, Department of Aerospace Engineering, 1983.

17. Boermans, L.M.M. and Blom, J.J.H., 'Low-speed aerodynamic characteristics of an 18% thick airfoil section designed for the all-flying tailplane of the M-300 sailplane'. Delft University of Technology, Dept. of Aerospace Engineering, report LR-226, 1976.

18. Pfenninger, W., 'Untersuchungen über Reibungsverminderungen an Tragflügeln, insbesondere mit Hilfe von Grenzschichtabsaugung'. Mitt. a.d. Inst. f. Aerodynamik, ETH Zürich Nr. 13, Verlag Gebr. Leeman & Co., Zürich, 1946.

19. Horstmann, K.H. and Quast, A., 'Widerstandsverminderung durch Blasturbulatoren'. DFVLR-FB 81-33, 1981.

20. Horstmann, K.H., Quast, A. and Boermans, L.M.M., 'Pneumatic turbulators - a device for drag reduction at Reynolds numbers below $5x\ 10^6$". Paper no. 20 in AGARD CP-365, Brussels, 1984.

21. Legendre, R., 'Décollement laminaire régulier'. Comptes Rendus 241, pp. 732-734, 1955.

22. Oswatitsch, K., 'Die Ablosungsbedingung von Grenzschichten'. In: Grenzschichtforschung/Boundary layer research. IUTAM Symposium, Freiburg/Br. 1957, Springer Verlag, pp. 357-367, 1958.

23. Batchelor, G.K., 'An introduction to fluid dynamics', Cambridge Univ. Press, 1970.

24. Smith, A.M.O., 'Improved solutions on the Falkner-Skan boundary layer equation'. Sherman M. Fairchild Fund Paper FF-10, Inst. Aero. Sci. 1954.

25. Stewartson, K., 'Further solutions of the Falkner-Skan equation'. Proc. Cambr. Soc, 50, pp. 454-465, 1954.

26. Goldstein, S., 'On laminar boundary layer flow near a position of separation'. Quart. J. Mech. Appl. Math. Vol. 1, pp. 43-69, 1948.

27. Liu, C.Y. and Sandborn, V.A., 'Evaluation of the separation properties of laminar boundary layers', the Aeron. Quarterly, Vol. XIX, Aug. 1968, part 3, pp. 235-242.

28. Ingen, J.L. van, 'Theoretical and experimental investigations of incompressible laminar boundary layers with and without suction'. Report VTH-124, Delft University of Technology, Dept. of Aerospace Engineering, 1965.

29. Mack, L.M., 'A numerical method for the prediction of high-speed boundary-layer transition using linear theory'. Paper nr. 4 in Aearodynamic analysis requiring advanced computers; NASA SP-347, 1975.

30. Wazzan, A.R., Okamura, T.T. and Smith, A.M.O., 'Spatial and temporal stability charts for the Falkner-Skan boundary layer profiles'. DAC 67086, Sept. 1968, McDonnel Douglas Corp.

31. Kummerer, H., 'Numerische Untersuchungen zur Stabilität ebener laminarer Grenzschichtstromungen'. Dissertation Technische Hochschule, Stuttgart, 1973.

32. Taghavi, H. and Wazzan, A.R., 'Spatial stability of some Falkner-Skan profiles with reversed flow'. Physics of Fluids, Vol. 17, no. 12, Dec. 1974, pp. 2181-2183.

33. Stratford, B.S., 'Flow in the laminar boundary layer near separation'. R and M 3002, 1957.

34. Stratford, B.S., 'The prediction of separation of the turbulent boundary layer'. Journal of Fluid Mechanics, Vol. 5, pt. 1, January 1959, pp. 1-16.

35. Horton, H.P., 'A semi-empirical theory for the growth of laminar separation bubbles. A.R.C.-CP 1073, 1967.

36. Gaster, M., 'The structure and behaviour of laminar separation bubbles'. In: AGARD CP4, Separated Flows, 1966, part 2, pp. 813-854.

37. Vogelaar, H., 'An experimental investigation of the laminar separation bubble on a Wortmann FX 66 S 196V1 wing section with and without a trip wire'. Engineering Thesis. Delft, September 1981.

38. Oudheusden, B. van, 'Experimental investigation of transition and the development of turbulence in boundary layer flow in an adverse pressure gradient'. Engineering Thesis, Delft, March 1985 (limited distribution).

39. Schubauer, G.B. and Skramstad, H.K., 'Laminar boundary layer oscillations and transition on a flat plate'. NACA Report 909, 1948.

40. Hall, D.J. and Gibbings, J.C., 'Influence of stream boundary layer transition'. Journal Mechanical Engineering Science, Vol. 14, no. 2, pp. 134-146 (1972).

41. Wells, C.S., 'Effects of free stream turbulence on boundary layer transition'. AIAA Journal, Vol. 5, No. 1, January 1967, pp. 172-174.

42. Spangler, J.G. and Wells, C.S., 'Effects of free stream disturbances on boundary-layer transition'. AIAA Journal, Vol. 6, No. 3, March 1968, pp. 543-545.

43. Volkers, D.F., 'Preliminary results of wind tunnel measurements on some airfoil sections at Reynolds numbers between $0.6 * 10^5$ and $5.0 * 10^5$. Memorandum M-276, Department of Aereospace Engineering, Delft University of Technology, 1977.

44. Boermans, L.M.M., Vries, J. de and Hegen, G.H., 'Preliminary results of wind tunnel measurements at low Reynolds numbers on airfoil section E 61'. Intern Rapport LSW 80-5, LSL, Department of Aerospace Engineering, Delft University of Technology, 1980.

45. Timmer, W.A., 'Experimental low speed aerodynamic characteristics of the Liebeck LA 5055 airfoil'. To be published as a Report by Department of Aerospace Engineering en Institute for Windenergy, Delft University of Technology.

46. Wentz, W.H. and Seetharam, H.C., 'Development of a fowler flap system for a high performance general aviation airfoil'. NASA CR-2443, 1974.

47. Crabtree, L.F., 'The formation of regions of separated flow on wing surfaces'. R and M 3122, 1959.